Chem Soc Rev

Design Principles for Creating Synthetic Underwater Adhesives

Journal:	*Chemical Society Reviews*
Manuscript ID	CS-SYN-03-2021-000316.R2
Article Type:	Review Article
Date Submitted by the Author:	20-Sep-2021
Complete List of Authors:	Narayanan, Amal; University of Akron, Polymer Science Dhinojwala, Ali; University of Akron, Department of Polymer Science Joy, Abraham; University of Akron, Polymer Science

Design Principles for Creating Synthetic Underwater Adhesives

Amal Narayanan, Ali Dhinojwala, and Abraham Joy**

School of Polymer Science and Polymer Engineering, The University of Akron, Akron, OH 44325, United States

Corresponding authors: *abraham@uakron.edu (A.J.) and ali4@uakron.edu (A.D.)

Abstract

Water and adhesives have a conflicting relationship as demonstrated by the failure of most man-made adhesives in underwater environments. However, living creatures routinely adhere to substrates underwater. For example, sandcastle worms create protective reefs underwater by secreting a cocktail of protein glue that binds mineral particles together, and mussels attach themselves to rocks near tide-swept sea shores using byssal threads formed from their extracellular secretions. Over the past few decades, the physicochemical examination of biological underwater adhesives has begun to decipher the mysteries behind underwater adhesion. These naturally occurring adhesives have inspired the creation of several synthetic materials that can stick underwater – a task that was once thought to be "impossible". This review provides a comprehensive overview of the progress in the science of underwater adhesion over the past few decades. In this review, we introduce the basic thermodynamics processes and kinetic parameters involved in adhesion. Second, we describe the challenges brought by water when adhering underwater. Third, we explore the adhesive mechanisms showcased by mussels and sandcastle worms to overcome the challenges brought by water. We then present a detailed review of synthetic underwater adhesives that have been reported to date. Finally, we discuss some potential applications of underwater adhesives and the current challenges in the field by using a tandem analysis of the reported chemical structures and their adhesive strength. This review is aimed to inspire and facilitate the design of novel synthetic underwater adhesives, that will, in turn expand our understanding of the physical and chemical parameters that influence underwater adhesion.

Keywords: Adhesives; underwater adhesion; bioinspired adhesion; interfacial interactions; cohesive network

1.0 Introduction

Adhesives are ubiquitous in modern society. They are used in everyday items such as sticky notes and adhesive bandages and are essential components in the manufacturing and assembly of modern appliances and electronics. Most everyday adhesives are liquids that have superior wetting properties and weak cohesive strength prior to their application. Once applied, the liquid cures to form a cohesively strong solid material that can bond substrates together. Prominent examples of adhesives that undergo this liquid-to-solid transition include Krazy glue®, Elmer's glue®, Loctite 430™, and Gorilla® Superglue. All of the commercially available glues work remarkably well in their appropriate setting. However, if water is present on the bonding interfaces most of these adhesives will fail instantly.[1–4]

Historically, much of the scientific developments in adhesive research were targeted towards engineering and household applications, where the chances of an encounter between the adhesive and water were prevented – at least until the adhesive had cured. But, the recent advancements in the field of automotive manufacturing, robotics, and healthcare call for the development of underwater adhesives – a new class of adhesive materials that can be spread, bonded, cured, and challenged underwater.[5,6] For example, in tissue engineering, adhesives are proposed to be the successor of sutures for sealing wounds and preventing the loss of blood and other body fluids.[7] In such biological settings, the presence of moisture is certain.[8–10] Therefore, the traditional adhesive materials that do not address the challenges brought about by water are ineffective in applications such as wound care and tissue fixation.[11]

The difficulty in creating adhesion between substrates underwater originates from the versatile mechanisms through which water can prevent or deteriorate adhesion.[12] In one mechanism, water molecules adsorb on the adhesive interfaces and reduce the molecular contact between the

adhesive and the substrate.[13] In another mechanism, water molecules diffuse into the bulk adhesive material and reduce (or chemically degrade) the cohesive strength of the adhesive material.[14] Because of these mechanisms, it has been difficult for chemists and material scientists to engineer underwater adhesive materials.

On the other hand, nature showcases a handful of elegant underwater adhesives.[15] Prominent examples include adhesive holdfasts known as byssal threads created by mussels that enable them to cling to rocks near intertidal zones,[16] the cement proteins secreted by sandcastle worms that aid them in assembling protective structures,[17] and the glue secreted by barnacles that allows them to attach to underwater rocks.[18] Within the past two decades, a fairly resolved picture of the biochemistry and adhesive mechanisms of these biological adhesives have been established,[19] which has led to a "bioinspired adhesive boom" for synthetic underwater adhesives.[20] Many of the studies on synthetic bioinspired adhesives show promising results in joining substrates underwater by overcoming the challenges brought by the presence of water.[1,2,28–31,3,21–27]

In this publication, we review the details of interfacial adhesion and the chemical design principles for creating bioinspired synthetic underwater adhesives. Compared to other excellent reviews,[5,6,38–41,10,11,32–37] we have focused on the role of chemistry in contact phenomena, viscoelastic dissipation, and interstitial water in biological and synthetic underwater adhesives. First, we introduce the basic thermodynamic and kinetic parameters involved in adhesion. Next, we describe the challenges brought by water when adhering substrates underwater and we present examples of biological adhesives and describe the adhesive mechanisms used to overcome the challenges brought by water. We then present a detailed review of synthetic underwater adhesives reported to date. Finally, we discuss some of the potential applications of underwater adhesives and the existing challenges in the field.

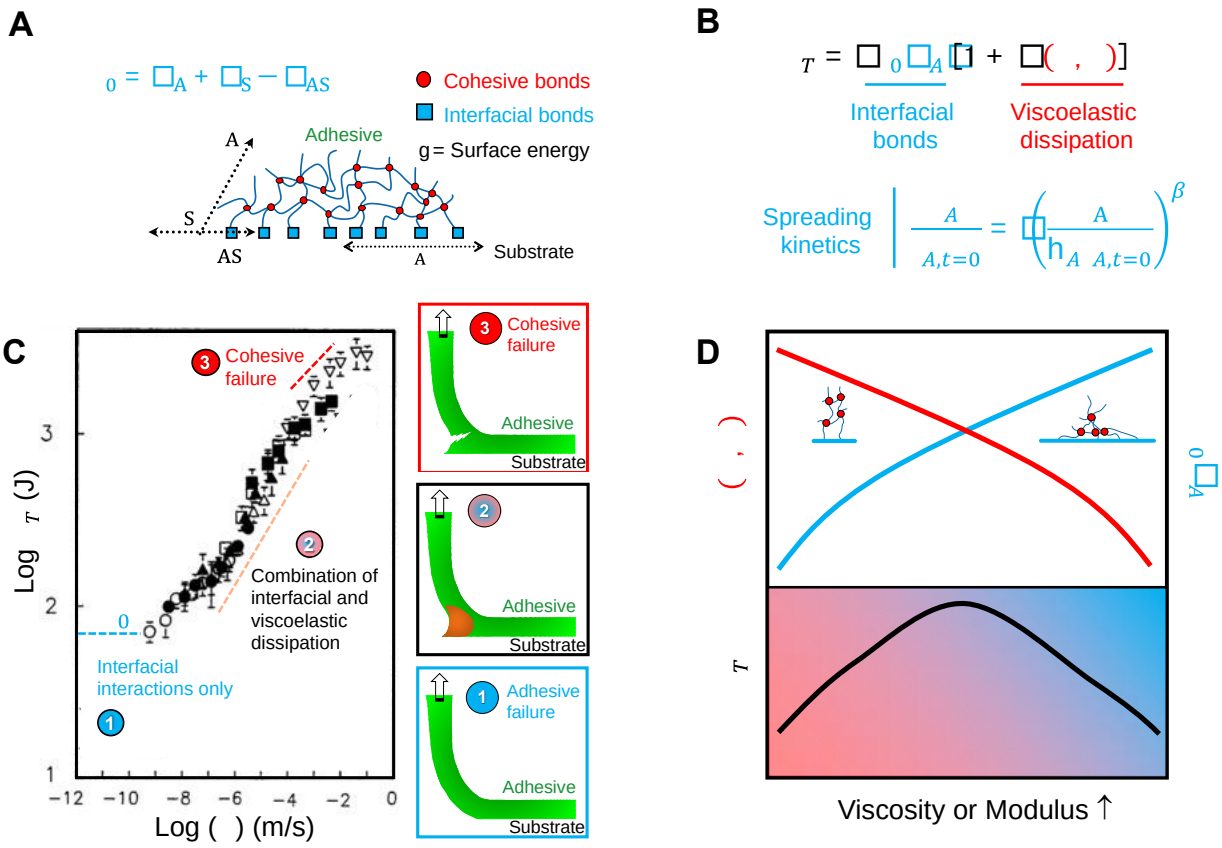

Figure 1. Introduction to the basic parameters that determine the adhesion of viscoelastic materials. (A) A depiction of the contact between an adhesive and the substrate with surface energies γ_A and γ_S, respectively. The interfacial energy of the newly formed interface is γ_{AS}. (B) The contact area (A_A) and the overall work of adhesion (U_T) (units of J) are determined by the thermodynamic work of adhesion (W_0) and the peel rate and temperature-dependent viscoelasticity ($f(R,T)$) of the adhesive. The W_0 is determined by the enthalpic interactions at the adhesive-substrate interface. The radius of the spreading front (r_A) of the adhesive is determined by γ_A and the viscosity of the glue (η_A). (C) The dependence of W_{ad} on the rate of the peel of a hydrocarbon elastomer. Reproduced from ref. 42 with permission from the American Chemical Society, copyright 1996. The mode of failure is dependent on peel rate and it transfers from adhesive to cohesive failure as the peel rate increases. The three zones can be visualized from the images on the right. (D) A qualitative understanding of the dependence of interfacial and viscoelastic components on the U_T. With the changes in the viscosity or the modulus of the adhesive, the interfacial and cohesive strength of adhesion changes with opposing trends. An optimal balance between interfacial and cohesive strengths is required to achieve maximum adhesive performance. Reproduced from ref. 43 with permission from the American Chemical Society, copyright 2015.

2.0 An Introduction to the Adhesion Strength of the Viscoelastic Materials

The adhesion energy between a viscoelastic material and a rigid substrate is determined by the combination of viscoelastic dissipation within the adhesive material (bulk cohesive strength) and the interfacial bonds (interfacial adhesion) at the contact interface (Figure 1).[42] A simplified empirical model for the relationship between the cohesive and adhesive strengths on overall adhesion strength is as follows:

$$W_{ad} = W_0 [1 + f(R,T)] \quad \text{Equation 1}$$

Where W_{ad} is the experimentally determined work of adhesion (in units of J/m^2), W_0 is the thermodynamic work of adhesion energy, R is the rate of peeling, and T is the experimental temperature. In Equation 1, W_0 is a function of the interfacial interactions and $f(R,T)$ represents the peel rate-dependent rheological functions that determine the cohesive strength.[42]

2.1 The Enthalpy of Interfacial Interactions and Adhesion Strength

The thermodynamic work of adhesion is defined by the following equation:

$$W_0 = \gamma_A + \gamma_S - \gamma_{AS} \quad \text{Equation 2}$$

where $\gamma_A + \gamma_S$ is the sum of the surface energies of the adhesive and substrate, and γ_{AS} is the interfacial energy at the contact between the adhesive and substrate.[44] In a seminal work, Fowkes showed that γ_{AS} is inversely proportional to the summation of the intermolecular enthalpic interactions ($\Delta H_{\text{interface}}$).[45] For molecules in the gaseous phase, dispersive interactions (ΔH_{D}) from Keesom dipole-dipole, Debye dipole-induced dipole, and London dispersion forces dominate the $\Delta H_{interface}$.[46–50] In liquids, the contribution of ΔH_{D} to $\Delta H_{\text{interface}}$ across nonpolar to polar liquids is

found to vary by only about 20%.[45,50,51] This indicates that for condensed phases such as liquids and solids, other interactions (acid-base interactions, ΔH_{ab}) such as hydrogen bonding primarily influence the $\Delta H_{interface}$.[45,50]

2.2 The Kinetics of Droplet Spreading and Adhesion Strength

As most common glues are initially in a liquid-like state, the contact area between the adhesive and substrate will depend on the efficiency of spreading of the liquid droplet. Therefore, the total peeling work, U_T (units of J) can be regarded as:

$$U_T = W_0 A_A [1 + f(R,T)] \quad \text{Equation 3}$$

where A_A is the area of contact between the surface and the adhesive.[42] This contact area is a function of the viscosity of the glue and the time for spreading. The advancement of droplet size (spreading kinetics) of the glue follows Tanner's law:

$$\frac{r_A}{r_{A,t=0}} = \left(\frac{\gamma_A t}{\eta_A r_{A,t=0}}\right)^{\beta} \quad \text{Equation 4}$$

where r_A is the radius of the spreading front on the substrate, $r_{A,t=0}$ is the initial radius of the glue, γ_A and η_A are the surface tension and viscosity of the glue, respectively; t is time, and β is a constant.[52] From Equation 2 and Equation 4 one can infer that the low value of γ_{AS} (higher interfacial interactions or low interfacial tension between the substrates) and low viscosity (higher spreading) increase the thermodynamic work of adhesion (W_0) (as shown in Figure 1B).

2.3 The Viscoelastic Dissipation and Adhesion Strength

The cohesive strength $f(R,T)$, of the adhesive is a variable that depends on the rate of peel at which the adhesive is removed. Studies by Gent have correlated the cohesive strength of the adhesive to the viscoelastic behavior of the adhesive materials.[42,53,54] At a higher peel rate and lower temperature, it was found that the adhesion behavior of simple hydrocarbon elastomers overlaps with the William-Landel-Ferry (WLF) model of the rate-temperature dependent polymer chain movements. Thus, the cohesive strength is attributed to the segmental mobility of the adhesive (Figure 1C).[53] For hydrocarbon elastomers, the second term of Equation 1, $f(R,T) = f(a_T T)$, where a_T is the ratio between the molecular motion of the adhesive at the glass transition temperature (T_g) and experimental temperature (T). Interestingly, the dependence of W_{ad} on the peeling rate (R) of the adhesive resembles the dependence of the storage modulus (G') on the angular frequency (ω) for soft elastomers. Also, at low peeling rates and high temperatures, the cohesive strength decreases significantly (Figure 1C). These relations between the molecular motion and cohesive strength imply that the second term of Equation 1 relates to the viscoelastic parameters of the adhesive material.[42]

Equations 3 and 4 show that the adhesion strength and viscoelastic properties of the adhesive are correlated through opposing contributions.[43] Equation 3 suggests that the higher viscosity of the adhesive will increase the contribution of $f(R,T)$ to the W_{ad}. However, Equation 4 implies that higher the viscosity, lower will be the spreading of the adhesive (Figure 1D). Therefore, to create adhesives with maximum W_{ad}, it is necessary to optimize *both* the adhesive and cohesive strengths.

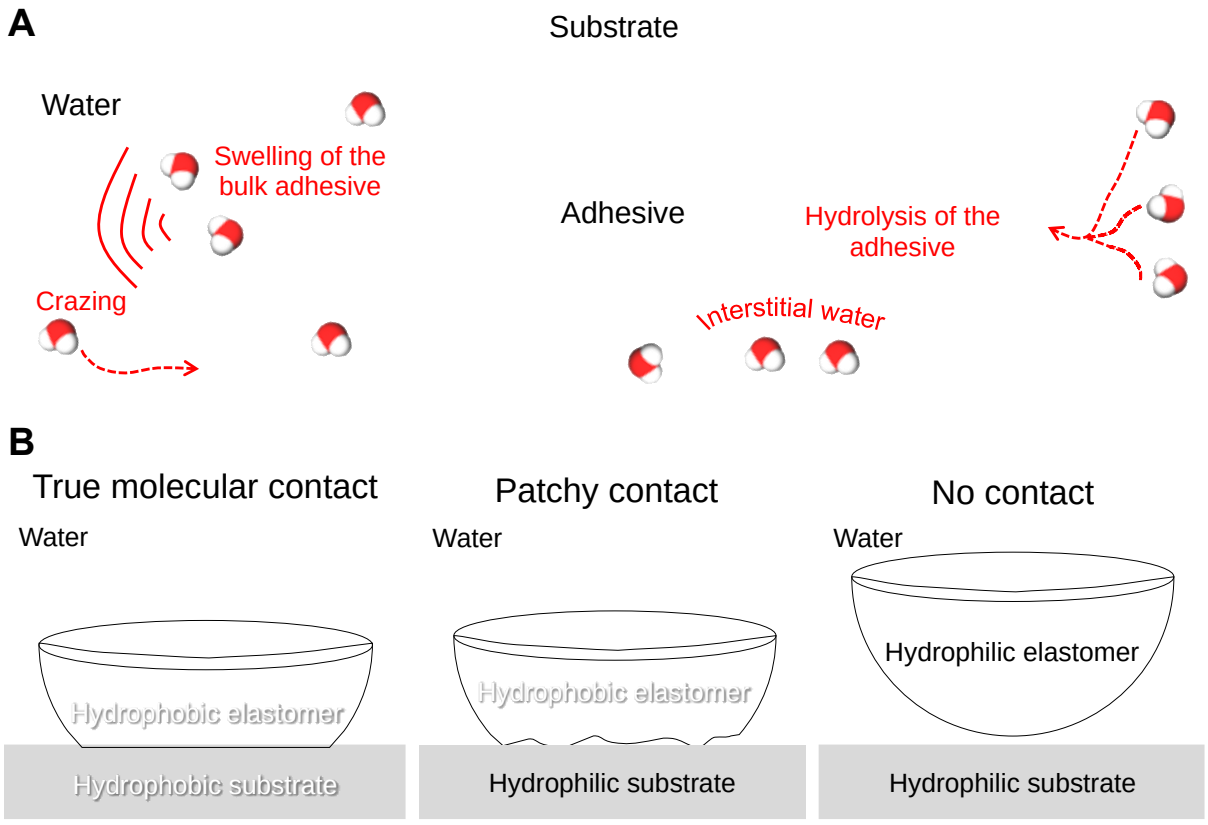

Figure 2. A summary of the consequences of the presence of water when adhering underwater. (A) A pictorial depiction of the mechanisms through which water deteriorates the adhesion strength. Water molecules disrupt the performance of adhesives by swelling and hydrolyzing the cohesive network of the adhesive, crazing to the interstices, and preventing the molecular contact between adhesive and substrate by adsorbing at interfaces. (B) A schematic description of the contact between hydrophilic and hydrophobic substrates underwater. The interface between two hydrophobic surfaces submerged underwater does not have water at the interface. The contact interface between the hydrophilic surface and hydrophobic elastomer forms a patchy contact that has two populations of interfaces. The first population is where the molecular contact is present between the adhesive and substrate. The second population is patches of trapped water that reduce the adhesion. The contact interface between two hydrophilic surfaces underwater possesses an interfacial water layer that prevents their underwater adhesion.

2.4 The Effect of Water on the Adhesion Strength

Although numerous adhesives with optimized interfacial and viscoelastic properties are produced globally for a spectrum of applications, the majority of these adhesives fail to work efficiently in moist air or underwater conditions.[1–4] This deterioration of adhesion in the presence

of water occurs through the following four pathways: (i) an adsorbed layer of water impedes the molecular contact between the adhesive and the substrate, (ii) the wicking and crazing of water molecules through the asperities of the substrate-adhesive interface, (iii) hydrolytic degradation of the adhesive, and (iv) plasticization of the cohesive network by water and swelling of the cured adhesive (Figure 2A).[12]

When applying an adhesive in an underwater setting, the conditions under which the substrate and adhesive are brought into contact can also determine the characteristics of the molecular contact. For example, the pressure at which the adhesive is applied can alter the kinetics of drainage of interstitial water. Because of the fluid present at the interface at low separation, a hydrodynamic force can develop at the interface. This force can be represented by Reynold's equation:

$$F_H = \frac{6\pi R^2 \eta v}{D} \qquad \text{Equation 5}$$

where R is the radius of the sphere, η is the viscosity of the liquid, and D is the closest distance separating the spherical adhesive from the flat substrate.[55,56] Frechette et al. measured the elastic deformation and hydrodynamic forces and provided insights regarding the dynamics of the contact interface due to the release of elastic energy.[57]

Among the major mechanisms that hinder adhesion, we focus on interstitial water, because interstitial water not only prevents molecular contact between the adhesive and the substrate but also weakens the interfacial adhesive bonds.[13,54,58,59] For example, the adhesion strength between epoxy and silica in dry conditions is 178 mJ/m^2, but it drops to -56.2 mJ/m^2 (

Table ***1***) in the presence of water.[58] The reduction in magnitude and the reversal in sign indicate the non-adhesive nature of these substrates underwater.[60] Most adhesives rely on electrostatically driven molecular interactions such as Coulombic, dispersive, and acid-base interactions. The polar nature of water directs these interactions towards itself and weakens the adhesive-substrate interfacial bonds.[45]

However, in water, hydrophobic interactions can facilitate underwater adhesion.[13,27,61–63] An example is the strong adhesion between two hydrophobic substrates underwater. The adhesion strength between two hydrophobic surfaces, polydimethylsiloxane (PDMS) and octadecyltrichlorosilane (OTS) underwater was found to be ~ 1.75-times higher than in dry conditions (

Table ***1***).[62] Chaudhury and Whitesides had proposed that the nature of adhesive contact between two substrates is a function of their corresponding interfacial energies in water.[13] In an underwater environment the two hydrophilic surfaces underwater tend to form a thick water bridge when they come into contact, and the contact between two hydrophobic surfaces develops a smooth molecular contact devoid of interstitial water. When a hydrophilic surface and a hydrophobic elastomer come into contact, a patchy contact is formed between the surfaces (as shown in Figure 2B).[64] This patchy contact has two types of interfaces: in some regions, the adhesive is in molecular contact with the substrate, while in other regions, the water molecules adhered to the hydrophilic substrate prevent molecular contact between the adhesive and the substrate. The adhesion strength in such patchy contacts is dependent on maximizing the regions

of molecular contact between the adhesive and substrate.[61,63] However, hydrophobic surfaces are susceptible to fouling in water and lose molecular interfacial contact in the presence of surfactants.[65]

Table 1. A comparison of the adhesion strengths (W_{ad}) measured between hydrophilic-hydrophilic (silica/epoxy) and hydrophobic-hydrophobic (PDMS/OTS) contacts in dry and underwater conditions.

Contacting interface	**W_{ad} (mJ/m^2)**	**Ref.**
Silica/epoxy (hydrophilic-hydrophilic contact) in dry conditions	178[a]	58
Silica/epoxy (hydrophilic-hydrophilic contact) in water	– 56.2[a]	58
PDMS/OTS (hydrophobic-hydrophobic) in dry conditions	40[b]	62
PDMS/OTS (hydrophobic-hydrophobic) in water	68[b]	62

W_{ad} is determined from [a]atomic force microscopy and [b]Johnson Kendall Roberts model contact adhesion measurements

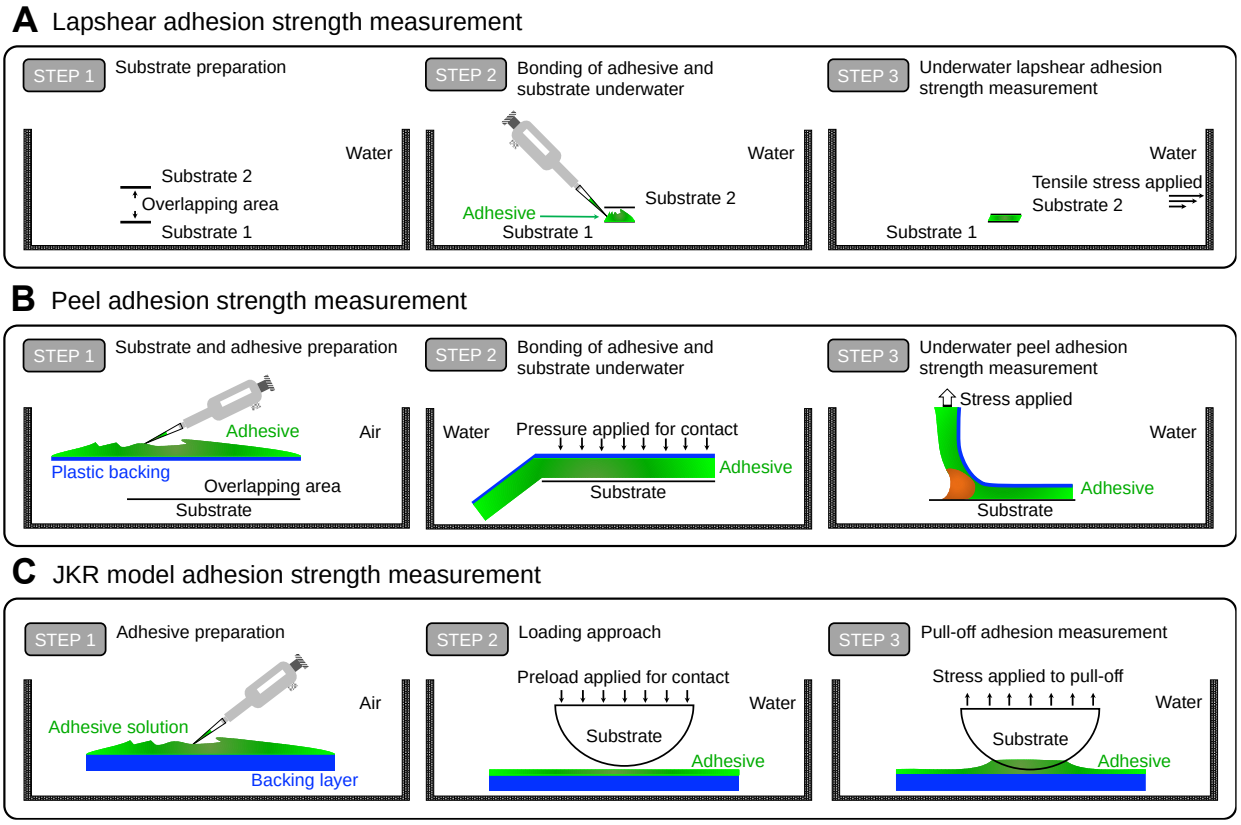

Figure 3. Summary of the commonly used experimental techniques for measuring underwater adhesion strength. The different steps involved in fabricating the samples for underwater adhesive testing using (A) lapshear adhesion strength measurement, (B) peel adhesion strength measurement, and (C) JKR model adhesion strength measurements are shown. In all the experimental geometries, the adhesive is brought in contact with substrates underwater. The ratio between cohesive and adhesive interactions is quantified differently across the adhesion strength measurement techniques. For example, cohesive interactions are the major contributor to lapshear adhesion measurements compared to interfacial interactions.

2.5 Experimental Techniques for Measuring Underwater Adhesion Strength

Adhesion force measurement methods such as lapshear strength measurement, the peel test, the tack probe test, and the Johnson Kendall Roberts (JKR) model have been used for measuring the adhesion strength of materials (Figure 3).[39] These methods are vastly different in their sample preparation and measurement sensitivity. Comparison of adhesion force measurements obtained using different techniques is not advisable, as the measured outcome might have a different ratio of contributions between interfacial and cohesive interactions. A detailed

insight into the common experimental techniques for adhesion strength measurement is described elsewhere.[39] In the following sub-sections, we introduce methods that have been adapted for underwater adhesion strength measurements.

2.5.1 Lapshear adhesion strength measurements

Lapshear adhesion strength measurements are considered to be the gold standard for measuring adhesion strength. Most literature examples follow ASTM D1002 guidance to obtain these measurements.[1,66] In ASTM D1002, the adhesive formulation is applied on two pieces of aluminum (Figure 3A). An overlapping area of 0.5 inch^2 is created between the two substrates and the adhesive is allowed to cure for a predetermined time. After curing, the substrates are pulled apart in a tensile geometry (crosshead speed = 1.3 mm/min). The force-distance curve (Figure 4A) obtained from the experimental results is then converted to lapshear strength or lapshear work of adhesion by using the following equations:

$$Lapshear\ strength, A_{Lap} = \frac{Maximum\ force\ load}{Lap\ joint\ area} \qquad \text{Equation 6}$$

$$Lapshear\ work\ of\ adhesion = \int Force \cdot Distance \qquad \text{Equation 7}$$

When testing the adhesive strength in lapshear strength measurement, the lap joint area is assumed to be constant. The lapshear adhesion strength for underwater adhesives typically varies between 10 – 3000 kPa.[1,20,27] Although lapshear adhesion strength measurement simulates the stress at adhesive interfaces, the major contributor to this measurement is the bulk cohesive interactions of the adhesive. In addition, the experimentally determined adhesion strength strongly correlates with the thickness of the adhesive coating.[67,68] In the geometry of the adhesion measurement, characterizing the failure mode of the adhesive is also problematic, as adhesive residues can be

found on the substrate even in adhesive failure.[69] Moreover, performing lapshear adhesion measurements underwater becomes more challenging since many of the adhesives cannot be spread underwater. Across the literature, there are wide variations in the procedures used for spreading, bonding, and curing the adhesive prior to obtaining the measurement.[1,3,25,27] These variations make it challenging to compare the strength across studies from different research groups.

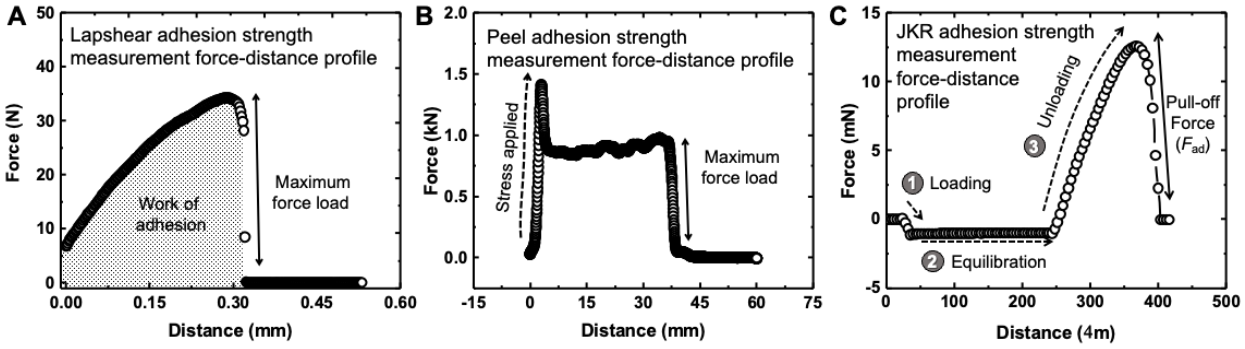

Figure 4. Examples of representative force-distance profiles obtained during (A) lapshear, (B) peel, and (C) JKR model underwater adhesion strength measurements. These force-distance profiles are converted to adhesion strength and work of adhesion. The lapshear strength measurements are commonly used for quantifying the adhesive strength of bulk polymer adhesives and coacervates. The peel adhesion strength measurement is commonly used for pressure-sensitive adhesives. The JKR model adhesion strength measurements are used for inferring interfacial adhesion strength of adsorbed polymer chains and elastomers.

2.5.2 Peel adhesion strength measurements

Peel tests are commonly performed for testing the adhesive strength of pressure-sensitive adhesives, and ASTM D3330 is recommended for preparing the adhesive joints and testing.[31,70] Typically, the adhesive is coated over a plastic backing (polypropylene or polyethylene terephthalate) and applied on an aluminum substrate (Figure 3B). The overlapping area is secured

by rolling a heavy (2 kg) rubber roller on the overlapping area. The adhesive joint is then peeled off at an angle using a force probe. The force-distance curve is recorded during the peel and the peel adhesion strength is obtained from the force-distance curve (Figure 4B). Different variants of peel tests such as 180°, 90°, static shear tests are used in the literature.[42,71,72] Typically, the peel adhesion strength is reported in the order of a few N/2.55 cm.

2.5.3 Johnson Kendall Roberts model adhesion measurements

A popular and more sensitive approach to measure the adhesion strength is to use Johnson Kendall Roberts (JKR) model adhesion measurements.[13,59,63,73–75] In a typical adhesion measurement, a hemispherical substrate is brought into contact with a flat surface (Figure 3C). Once the contact reaches a predetermined load and equilibration time, the substrates are pulled away from each other, and the adhesion force is recorded using sensitive force probes. JKR model adhesion measurements can be performed using a custom-built piezo setup,[62,63] a surface force apparatus,[74,76,77] or an atomic force microscope.[73,78] From the force-distance curve (Figure 4C), the adhesion strength (W_{ad}) can be determined using the JKR equation as follows:

$$W_{ad} = \frac{F_{ad}}{1.5\,\pi\,R_l} \qquad \text{Equation 8}$$

where F_{ad} is the pull-off force and R_l is the radius of the hemispherical lens. When performed at low contact or retraction rates, the adhesion strength measured using the JKR model corresponds to the interfacial interactions.[13,61–63] Typically, the adhesion strength measured for the contact between a hard (substrate) and a soft (adhesive) is on the order of 1-100 mJ/m^2.

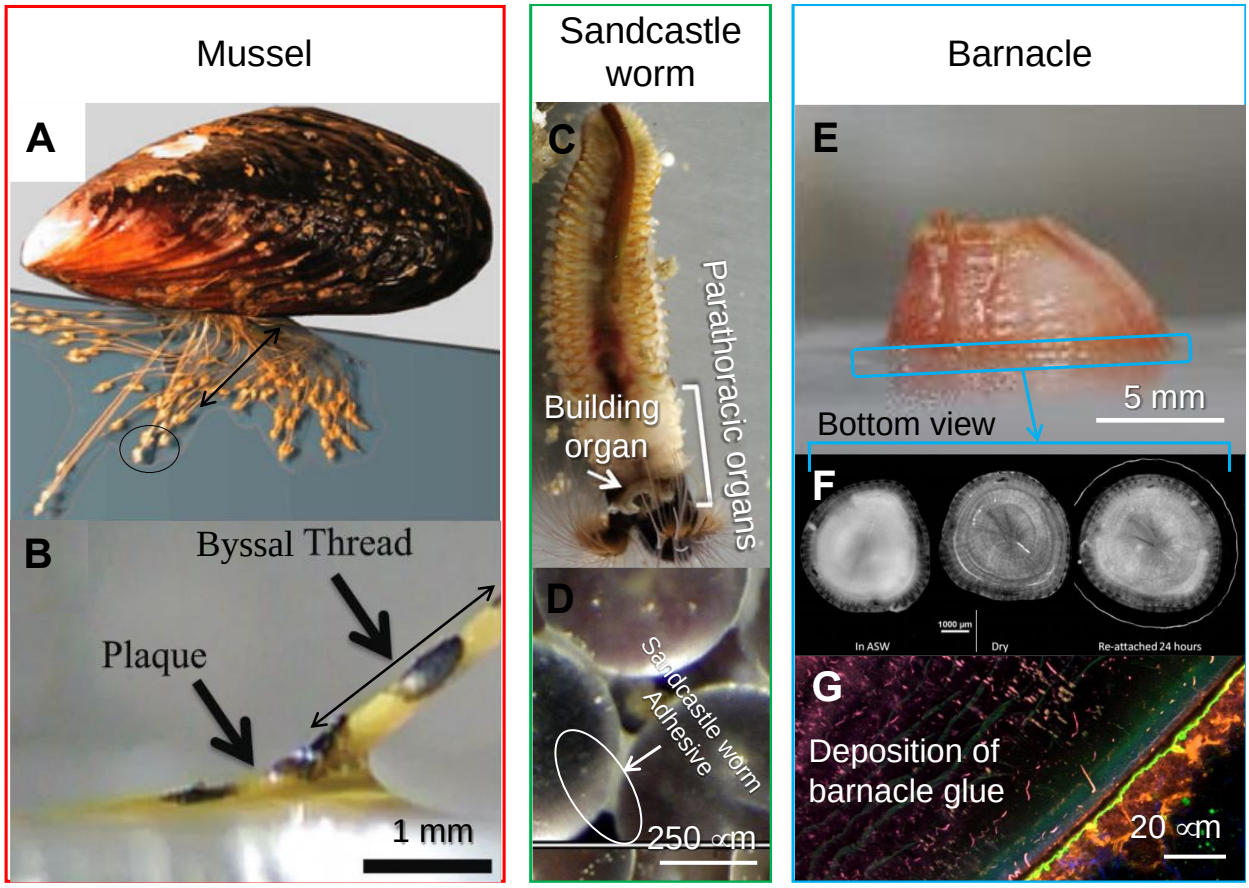

Figure 5. Three marine organisms that produce extracellular underwater adhesive secretions. (A) A mussel adhered to a substrate using its byssal threads. Reproduced from ref. 79 with permission from the Company of Biologists LTD, copyright 2017. (B) A magnified image of one mussel adhesive thread. A clear distinction between adhesive plaque and the thread region can be observed. Reproduced from ref. 80 with permission from the Royal Society of Chemistry, copyright 2015. (C) The parathoracic organs of the sandcastle worm contain the secretory glands and the building organ that assembles the tubular structure. Reproduced from ref. 81 with permission from the Elsevier, copyright 2016. (D) A structure made by sandcastle worm with their adhesive using microscopic glass beads. Reproduced from ref. 82 with permission from the Elsevier, copyright 2010. (E) The picture of an adult barnacle and the (F) bottom view of the contact between barnacle and surface (left to right: normal, dried, and rehydrated contacts). Reproduced from ref. 83 with permission from the John Wiley and Sons, copyright 2012. (G) A cross-sectional fluorescent microscopic image of the deposition of the barnacle glue. Reproduced from ref. 84 with permission from the WILEY-VCH Verlag GmbH & Co. KGaA, Weinheim, copyright 2018.

3.0 Natural Underwater Adhesive Engineers

Organisms such as mussels, sandcastle worms, caddisfly larvae, and barnacle as well as bacteria in the genus *Caulobacter* exhibit adhesive mechanisms that enable their lifecycle in aqueous environments (Figure 5).[15,19,60,79] For example, adult barnacles attach themselves to rocks along tide-swept shores with distinct protein recipes while they metamorphose from a free-swimming cyprid phase to a sessile adult barnacle phase.[85] The adult barnacle exoskeleton remains permanently attached to rocks even after the end of its lifecycle (Figure 5 E-G).[86] Although these organisms belong to different phyla, mussels, sandcastle worms, and caddisfly larvae secrete a cocktail of distinct proteins that enable them to sustain their life in aquatic environments.[19] The detailed review of the adhesive mechanisms of the organisms can be found elsewhere.[5,15,19,79,87] Inspired by numerous examples of biological underwater adhesives, synthetic underwater adhesives have been developed.[5,6,20,32] Among these adhesives a majority of the underwater adhesives are created with inspiration from the adhesive mechanisms of mussels and sandcastle worms. Therefore, in this section, we limit the review to an introduction to the adhesive mechanisms of mussels and sandcastle worms adhesives and synthetic underwater adhesives inspired by these organisms.

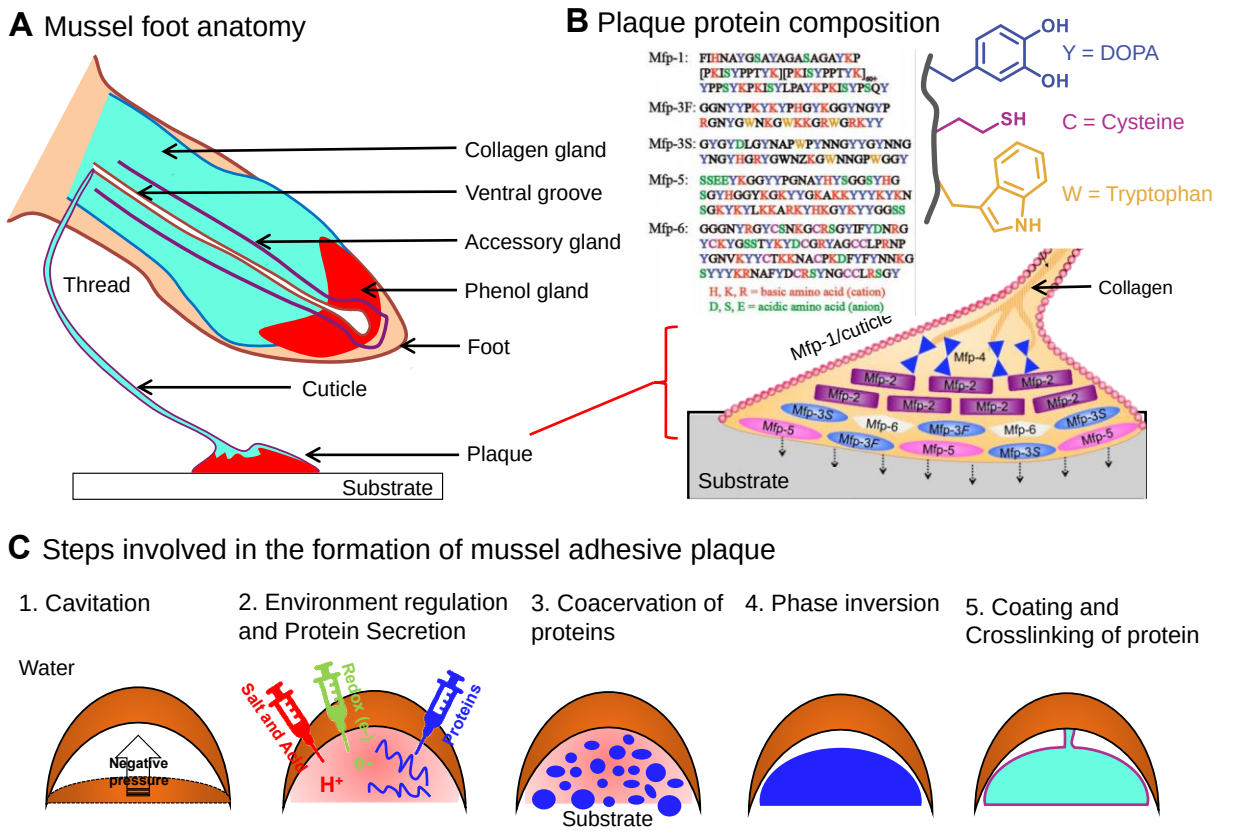

Figure 6. An overview of the mechanism of the mussel adhesion. (A) The anatomy of the mussel foot containing the secretory glands that secrete the proteins necessary for the formation of the mussel byssal thread. (B) A pictorial representation of the proteins found in the mussel byssal thread with a list showing the amino acid composition of the proteins found in the plaque. Reproduced from ref. 6 with permission from the Royal Society of Chemistry, copyright 2020. (C) Proposed steps involved in the formation of mussel byssal thread. The biochemical events near the distal region of the mussel foot are shown. The first step is proposed to be a cavitation event where the mussel foot exerts a negative pressure to drive water away from the surface before the secretion of the proteins. Later, the proteins that regulate the biochemical processes of adhesion and curing are secreted. The adhesive proteins undergo coacervation and phase inversion before the formation of coating and byssal thread maturation.

3.1 Underwater Adhesion of Mussels

Mussels are sessile organisms commonly found in inter-tidal zones (Figure 5A). To overcome the lift-off forces caused by wave action, each mussel creates more than 50 adhesive holdfasts knowns as the byssal threads.[88] In a time interval of a few minutes, mussels secrete at

least 20 foot proteins (Mfp) through the ventral grove located in the core of the mussel foot (Figure 6A and Figure 6B). Mfps undergo a series of physicochemical changes to become the final byssal threads.[89] Waite suggests that the formation of the byssal thread involves at least five following steps: (i) first, the distal region of the mussel foot creates a cavity with negative pressure near the substrate, then (ii) the chemical environment inside the cavity is regulated by manipulating the pH, ionic strength, and redox potential, followed by the (iii) secretion of partially soluble proteins (coacervates) that later (iv) undergo water/protein phase inversion. Finally, the mussel foot assembles (v) the Mfp-1-based coating over the phase inverted immature byssal thread, which then solidifies through mineral and enzyme-assisted crosslinking reactions and form mature adhesive byssal threads.[79]

Table 2. Summary of the location, molar mass, structure, DOPA content, and adhesion strength to mica (W_{ad}, measured using surface force apparatus) of the proteins found in the mussel byssal thread. Reproduced from ref. 6 with permission from the Royal Society of Chemistry, copyright 2020.

Protein	Location	Molar mass (kDa)	Structure	DOPA content (mol%)	W_{ad} (mJ/m^2)
Mfp-1	Cuticle	~ 110	Disordered	15	1
Mfp-2	Plaque core	45	Disordered	5	1
Mfp-3f	Plaque-substrate interface	6	Disordered	20	6
Mfp-3s	Plaque-substrate interface	6	Disordered	10	3
Mfp-4	Plaque core	90	Disordered	2	0
Mfp-5	Plaque-substrate interface	11	Disordered	30	15
Mfp-6	Plaque-substrate interface	12	Disordered; beta	5	0.5
Mfp-7	Plaque core	35	--	0.2	--

Collagen (preCOL-D, -P, -NG)	Thread core	240 (trimer)	Structured	0.1	--

The byssal threads of mussels consist of an adhesive plaque near the substrate-holdfast interface and a collagenous thread that connects the plaque to the mussel (Figure 6B).[88,90,91] The proteins found across these two segments are vastly different in their structure and physicochemical properties (Figure 6B). Among the 20 proteins that have been identified in the byssal thread, Mfp-3f, -3s, -5, and -6 are found at the plaque-substrate interface. These interfacial proteins are proposed to play crucial roles in maintaining the adhesive strength of the mussel byssal threads.[76,92–97] Interestingly, these four proteins found at the interface have low molar mass (Table 2, 5 – 12 kDa) compared to the other proteins found in the byssal thread.[79] It can be hypothesized that the low molar mass of the proteins found near the plaque-substrate interface reduces the viscosity of the adhesive and improves the interfacial interactions as indicated from Equation 3.[54]

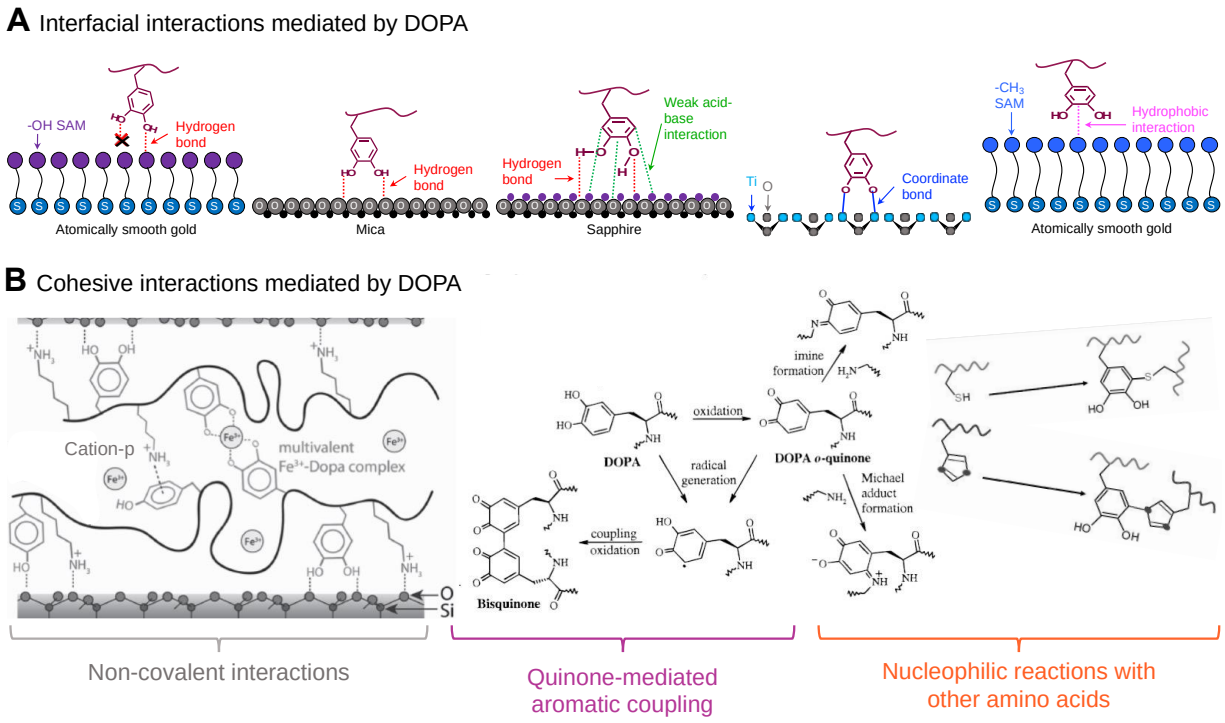

Figure 7. Summary of the mechanisms through which DOPA units contribute to the adhesive and cohesive strength of Mfps and their mimics. (A) Interfacial and (B) cohesive strengthening mechanisms of DOPA. DOPA molecules are proposed to interact at the interfaces via single hydrogen bond (to -OH self-assembled monolayers, SAM), bidentate hydrogen bonds (to mica surfaces), weak and strong acid-base interactions (to hydroxylated surfaces), metal-coordinate bonds (to metallic surfaces), and hydrophobic interactions (to organic surfaces). DOPA molecules can form crosslink points in the cohesive network by multivalent coordination bonds, cation-π interaction, and covalent bonds by quinone-mediated aromatic coupling and reacting with other nucleophilic amino acids variable groups. Reproduced from ref. 98 with permission from the American Chemical Society, copyright 1998. Reproduced from ref. 74 with permission from the WILEY-VCH Verlag GmbH & Co. KGaA, copyright 2015.

3.1.1 DOPA-mediated interfacial interactions and interstitial water removal

Perhaps the most recognized feature of the Mfps is the post-translational modifications found in their amino acids.[16,99–102] One of the most discussed post-translational modifications in Mfps is the conversion of tyrosine units to 3,4-dihydroxyphenylalanine (DOPA).[79] DOPA is found in substantial amounts (5 – 30 mol% DOPA) in the Mfps that form the cuticle (Mfp-1) around the byssal thread and the plaque-substrate (Mfp-3s, -3f, and -5) interface (Table 2). However, DOPA

is found in low amounts (2 – 5 mol% DOPA) in the Mfps that form the plaque core (Mfp-2 and Mfp-4).[79] A wide variety of molecular-level adhesive mechanisms for Mfps are proposed based on the unusual presence of DOPA units in the adhesive proteins. DOPA units consist of a catechol group (3,4-dihydroxybenzene, referred to as DOPA in this review) that is proposed to improve the interfacial bonding and cohesive strength of the adhesive byssal threads.[6] By studying the adhesive behavior of Mfps and their analogs, it is proposed that the dihydroxyl groups in DOPA form bidentate hydrogen bonds to the mica surface,[73,103,104] multimodal acid-base interactions to hydroxylated Al_2O_3 surface,[63,105] and coordinate bonds to metallic surfaces.[73,93,106,107] Meanwhile, the phenyl groups of DOPA can form interfacial bonds through hydrophobic, π-π interactions, and weak acid-base interactions (Figure 7A).[94,97,105]

Using ATR-IR spectroscopy in an adsorption geometry, Wei et al. showed that the Mfp-3s-mimicking peptides with DOPA units dry the interstitial water more efficiently than the tyrosine variant on TiO_2 and hydroxyapatite surfaces.[108] Akdogan et al. studied the changes in diffusivity of interfacial water on polystyrene and silica surfaces when adsorbed with Mfp-3s, Mfp-3f, Mfp-1, and Mfp-5 using Overhauser dynamic nuclear polarization (ODNP) relaxometry. Interestingly, the relatively hydrophobic protein - Mfp-3s, showed the capability of displacing interstitial water while adsorbing onto polystyrene surface.[109] Notably, the relatively hydrophilic proteins Mfp-3f, Mfp-1, and Mfp-5 did not alter the dynamics of interstitial water. It was found that none of the proteins perturbed the interstitial water on hydrophilic silica surfaces.

3.1.2 DOPA-mediated cohesive interactions

In addition to the various mechanisms through which DOPA is proposed to improve interfacial interactions, DOPA units can also enhance the cohesive strength of the adhesive through various physical and chemical bonding (Figure 7B). DOPA enhances the cohesive strength of

Mfps by physical interactions such as DOPA-DOPA hydrogen bonding and DOPA-lysine cation-π interactions.[74,110,111] Since the adhesives are secreted in marine water where a substantial amount of minerals are present, DOPA units in Mfps form coordinate complexes with metal centers present in water.[112] Often, 2-3 DOPA molecules form bidentate coordination complexes with one metal center in the protein structure and act as crosslinking points that improve the storage modulus (G') of the Mfps.[74] The dynamic nature of this DOPA-metal coordinate complex also helps in providing viscoelastic dissipation and provides toughness to Mfps.[113–115] The DOPA units are noticeably active to changes in redox and pH of the active environment. At pH > 9 or in the presence of oxygen, DOPA converts to quinone which has an electrophilic site available for nucleophilic reactions with amino acids such as lysine and cysteine to form covalently crosslinked protein networks.[95] The semiquinones formed from the oxidation of catechol units can also undergo aromatic cross-coupling and form crosslinking points (Figure 7B).[116]

3.1.3 Disordered structure of Mfps and coacervation

Many proteins found in nature adopt secondary structures to protect their active sites and maintain their functionality.[117] On the contrary, Mfp-3s and -5 do not possess secondary structures and resemble an extended coil with intrinsically disordered domains (IDRs, Table 2).[79,118,119] Under suitable conditions, such disordered proteins can undergo a liquid-liquid phase separation (LLPS) process, known as *coacervation*.[120] Proteins that display coacervation will form two distinct phases in aqueous solutions, namely, dilute and dense phases. The dense phase contains more protein compared to the dilute phase.[121] Notably, the dense phase is denser than water, with viscosity optimal for efficient spreading, and shows low interfacial tension underwater.[122] Wei et al. found that Mfp-3s undergo single-component coacervation at pH = 3 – 6 and NaCl concentration = 0.1 – 0.6 M.[123] This coacervation behavior is proposed to help mussels coat

underwater surfaces with adhesive primers (Figure 6C). While other Mfps also exhibit IDRs in their protein structure,[6] no studies exploring their coacervation behavior have been reported in the literature.

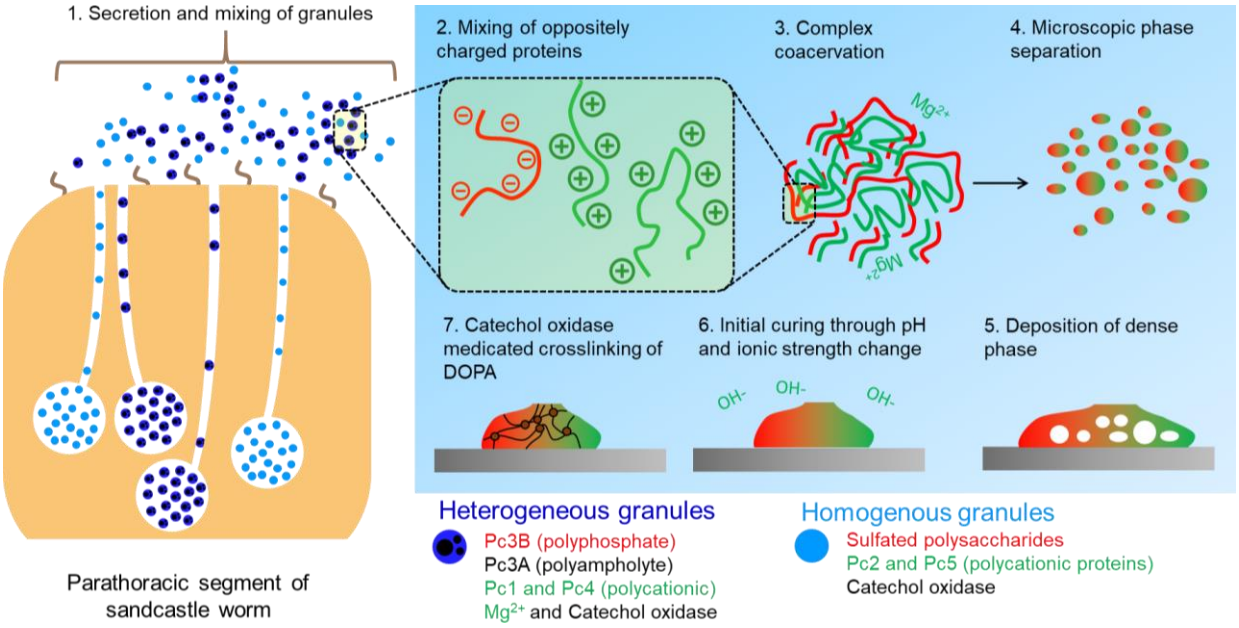

Figure 8. An overview of the underwater adhesive mechanism of the sandcastle worm is shown at different length scales. The homogeneous and heterogeneous adhesive granules are initially secreted from the secretory cells in the parathoracic glands of the sandcastle worm. The components in the granules are shown at the bottom right. The granules are mixed by the cilia which leads to complex coacervation of the oppositely charged proteins and polysaccharides. The dense phase formed from the complex coacervation is initially cured by the changes in the environmental pH and ionic strength. The DOPA-based final curing of the adhesive is mediated by catechol oxidase.

3.2 Underwater Adhesion of Sandcastle Worms

Sandcastle worms, often found on turbulent shoresides, protect themselves with elaborate structures they construct from adhering together mineral particles,.[124] To build the sandcastle, these polychaete tubeworms stick minerals together with their intrinsically generated underwater glue

(Figure 5C and Figure 5D).[125] The glue is rich in proteins and metal salts and is secreted as homogeneous and heterogeneous granules from secretory cells found near the parathoracic segments of the worm (Figure 8). Six sandcastle worm adhesive protein compositions have been characterized to date.[81] Four of the proteins (Pc1, Pc2, Pc4, and Pc5) are polybasic and are rich in amino acids such as lysine, histidine, and tyrosine. The other two proteins are Pc3A, (which is polyacidic) and Pc3B (which is a polyampholyte). Interestingly, the polyacid nature of Pc3A originates from the post-translational phosphorylation of an unusual amount (≈ 90 %) of serine units into phosphoserine. The tyrosine units in Pc1 and Pc2 are modified to DOPA units (similar to that of interfacial Mfps. In addition to the proteins, the sandcastle worm glue contains Ca^{2+} and Mg^{2+} ions, sulfated polysaccharides, and catechol oxidase.[15,82,126–128]

3.2.1 Complex coacervation of sandcastle worm adhesives

The sandcastle worm glue precursors are rich in cationic and anionic groups (≈ 40 mol%).[126] It is proposed that a condensation between these cationic and anionic proteins occur at the paddle-shaped cilia covering the building organ of the sandcastle worm (Figure 5C and Figure 8). Such complexation between the oppositely charged proteins forms a complex coacervate phase just before the application of the glue. Hence, the complex coacervation is suggested to be a crucial step in the initial adhesion of the sandcastle worm structures.[82] Unlike Mfp-3s, the driving force for the complex coacervation of weak polyelectrolytes like polyphosphate (Pc3A) and polylysine (Pc2) is enthalpic interactions (electrostatic) between oppositely charged macromolecules.[129,130] Nevertheless, similar to the single-component coacervation of Mfp-3s, the complex coacervation also creates a water-immiscible dense phase that may be applied as an underwater adhesive.

3.2.2 Two-step curing of the sandcastle worm adhesive

The sandcastle worm adhesive is proposed to undergo a two-step curing process for a permanent setting (Figure 8).[82,131] In the first step, the liquid-like complex coacervate combines with divalent ions (Mg^{2+} and Ca^{2+}) and responds to differences in pH between the secretory system (pH < 6) and seawater (pH > 8). Since the mode of interaction between proteins in this complex coacervate is electrostatic, the interfacial and viscoelastic properties of complex coacervates are highly sensitive to changes in ionic strength and pH.[81] Therefore, the sandcastle worm adhesives solidify remarkably fast (first curing time < 30 s) once applied in seawater.[17] In the second step, DOPA units are oxidized by catechol oxidase found in the adhesive granules of the sandcastle worm. This oxidation process leads to the phase transition of the glue from a white semi-solid to a tough, leathery, and brownish solid, indicating the *o*-quinone-mediated crosslinking reactions of DOPA units in Pc1 and Pc2 (Figure 7B).[81] The combination of interfacial wetting properties of the complex coacervation and the cohesive strength derived from the two-step solidification process is responsible for the performance of sandcastle worm adhesives underwater.

Table 3. Classification of synthetic bioinspired adhesives based on the fabrication and testing of adhesive joints. Representative examples of individual classes can be found in the references cited.

Classification of bioinspired adhesive	Steps involved in creating the adhesive joint and their wet/dry conditions				Ref.
	Spreading	Bonding	Curing	Testing	
Dry adhesive	Dry	Dry	Dry	Dry	132–137
Water-resistant	Dry	Dry	Dry	Underwater	138–141
Wet adhesive	Wet	Wet	Humid	Wet/Dry	98,142–145
Underwater adhesive	Underwater	Underwater	Underwater	Underwater	2,21,27,31,146,147

4.0 Bioinspired Synthetic Underwater Adhesives

Exciting discoveries over the past few decades have provided a deeper understanding of the temporal, biological, chemical, and physical mechanisms of the underwater adhesion of aquatic organisms.[79,81] The biochemical and biomechanical studies of underwater biological adhesives over the past four decades have drafted design guidelines for synthetic chemists and engineers to use in creating adhesives that stick underwater.[5,6,73,80,89,93,96] For example, inspired by the presence of DOPA units in Mfp and Pc, a wide variety of bioinspired adhesives have been created by appending DOPA units on various oligomer and polymer backbones.[6,92,148] This method dates back to the pioneering study by Yamamoto in 1987 where a poly(decapeptide) containing 10 mol% DOPA showed an adhesion strength of ≈ 2.7 MPa when used to adhere two iron plates.[142] Similarly, Yu and Deming created an adhesive formulation of lysine-DOPA copolypeptide and tyrosinase, that showed a maximum lapshear adhesion strength (A_{Lap}) of ≈ 4.7 MPa when adhering together two Al_2O_3 plates.[149]

These initial studies have created a "bioinspired adhesive boom" over the past decade, which has led to a wide variety of synthetic bioinspired adhesives with better adhesion than the mussel adhesive plaque.[20] However, many of these studies were not able to emulate the elegance of the underwater adhesives of mussels or sandcastle worms because (i) all the steps involved in adhesion were not carried out underwater, (ii) use of toxic organic solvents or plasticizers in the adhesive formulation, and (iii) impractical curing time (some studies with > 1 h curing time). The elegance of mussel and sandcastle worm adhesion is the ability of these organisms to carry out all the steps involved in adhesion, i.e., spreading, bonding, and curing while underwater.[19] In the past few years, researchers have demonstrated the ability to create adhesives that perform all the steps

of adhesion underwater (Table 3). In this review, we have only considered the literature examples in which all the steps of the adhesion process were performed underwater.

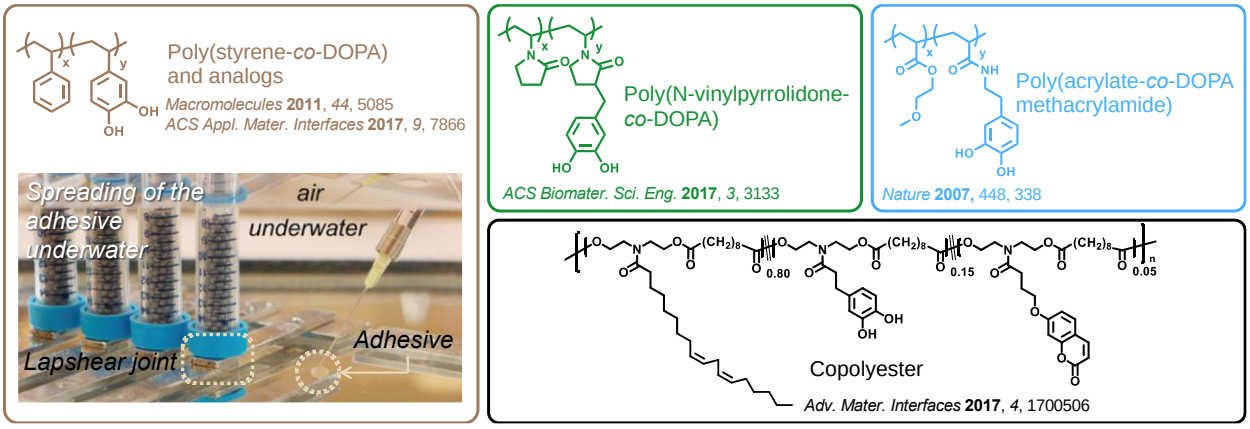

Figure 9. Bioinspired synthetic underwater adhesives can be broadly categorized into three classes: Bulk polymers, Coacervates and Tacky Adhesives. Few of the examples of the underwater water adhesives in the Bulk polymers category – materials where the underwater adhesion depends on the liquid → solid transition of the polymer or the solution are shown here. Reproduced from ref. 1 with permission from the American Chemical Society, copyright 2011.

It is well-established that DOPA molecules can interact with surfaces to improve interfacial interactions (Figure 7).[63,73,104,106,107] Also, the formation of DOPA-metal complexes and oxidative crosslinking of DOPA underwater enhance the cohesive strength of the material (Figure 7).[95,112,150] This versatility of DOPA for improving the overall adhesion strength has motivated researchers to design underwater adhesives by synthesizing polymers functionalized with DOPA (or catechol).[5,6,36,92] These adhesives have a broad range of adhesive mechanisms, material properties, and adhesion strength. Since the adhesion strength measurement technique of choice depends on the material properties of the adhesive formulation, in this review we classified the underwater adhesives based on their material properties and the geometry of adhesion strength measurements used in the report. Broadly, bioinspired underwater adhesives can be categorized into three major

categories (Figure 9, Figure ***11***, and Figure ***12***). The first category is polymers that are spread (or injected) on surfaces dissolved with or without organic solvents – bulk polymer underwater adhesives. These adhesives are cured via polymer chain entanglements, solvent evaporation, oxidation reactions, or crosslinking reactions. The second category of underwater adhesives is the liquid-like dense phase adhesives formed from the coacervation process which is later cured through environment switching and crosslinking reactions. Typically, lapshear adhesion strength measurements are used in testing the adhesion strength of these two classes of materials. The third category is tacky adhesives that are thermoplastic elastomers or crosslinked networks. The adhesion strength is typically measured using a contact adhesion geometry for this class of materials. In the following section, we will review these three categories of underwater adhesives (Table 4).

Table 4. Summary of the underwater adhesive formulations, curing mechanism, time (t), and temperature (T), maximum lapshear adhesion strength (A_{Lap}), and the corresponding references.

Polymer	**Other reagents**	**Curing conditions**			**A_{Lap} (MPa)**		**Ref**
		Mechanism	***t*** **(h)**	***T*** **(ºC)**	**Dry**	**Under water**	
		Bulk polymers					
Poly(styrene-*co*-$^{+}$NEt$_3$-*co*-DOPA)	$Bu_4N^+(IO_4^-)$, methanol and $CHCl_3$	Oxidation of DOPA and chain entanglement	24	50	2.8 ± 0.6	0.4 ± 0.2	[1]
Poly(styrene-*co*-DOPA)	Methanol and $CHCl_3$	Autoxidation of DOPA and chain entanglement	24	r.t.	3 ± 1	2.2 ± 0.9	[2,136]

Poly(MMA-*co*-DOPA-*co*-phosphate)	Acetone, water, and $Bu_4N^+(IO_4^-)$	Oxidation of DOPA and chain entanglement	24	r.t.	2.4	0.5	[69]
(DOPA-PLA) copolyester	$Bu_4N^+(IO_4^-)$ and acetone	Oxidation of DOPA and chain entanglement	24	37	2.6 ± 0.4	1.0 ± 0.3	[151]
(DOPA-Coumarin-Hydrocarbon) copolyester	None	Photocrosslinking of coumarin	0.2	r.t.	0.87 ± 0.08	0.65 ± 0.09	[27]
DOPA-bis(4-glycidyloxyphenyl) alternating copolymer	$FeCl_3$, methanol, and $CHCl_3$	Oxidation of DOPA, metal coordination, and chain entanglement	168	r.t.	n.d.	0.91 ± 0.08	[152]
Poly(DOPAmethacrylamide-*co*-ethylmethoxy acrylate)	$FeCl_3$, methanol, and $CHCl_3$	Oxidation of DOPA, metal coordination, and chain entanglement	24	r.t.	0.9	0.4	[22]
DOPA-ethylmethoxy copolymethacrylamide	$FeCl_3$, methanol, and $CHCl_3$	Oxidation of DOPA, metal coordination, and chain entanglement	24	r.t.	1.1	0.6	[22]
poly(N-vinylpyrrolidone-*co*-DOPA)	$FeCl_3$, methanol, and $CHCl_3$	Oxidation of DOPA, metal coordination, and chain entanglement	24	r.t.	1.3	1.3	[22,153]
Poly(DOPA-*co*-butylacrylate)	Methanol and $CHCl_3$	Autoxidation of DOPA and chain entanglement	144	r.t.	0.7	0.5	[3]

Poly(pyrogallol -*co*- butylacrylate)	Methanol and $CHCl_3$	Autoxidation of DOPA and chain entanglement	144	r.t.	3	1.35 ± 0.17	[3]
		Coacervates					
Poly(phosphate -*co*-DOPA) and Polyamine	Water, Ca^{2+}, $NaIO_4$, PEGDA, and free-radical initiators	Oxidation of DOPA, crosslinking of PEGDA, and environment switching	24	r.t.	n.d.	0.97 ± 0.26	[21]
Poly(phosphate -*co*-DOPA) and Gelatin-amine	Water, Mg^{2+}, and $NaIO_4$	Oxidation of DOPA and environment switching	24	r.t.	n.d.	0.75	[25]
Rmfp and hyaluronic acid	Water	Autoxidation of DOPA	24	r.t.	4.0 ± 0.5	0.24 ± 0.10	[147]
PAH and TPP	Water and salt	Complexation of charged groups	4	r.t.	n.d.	0.4	[29]
DOPA-conjugated elastin	Water	Autoxidation of DOPA	24	37	2.6 ± 0.6	0.24 ± 0.09	[28]
(DOPA-Coumarin) non-ionic copolyester	Water	Photocrosslinking of coumarin	0.2	r.t.	n.d.	0.10 ± 0.02	[24]

4.1 Bulk Polymer Underwater Adhesives

Wilker and coworkers have carried out a series of pioneering studies in optimizing the adhesion of DOPA-conjugated styrenic copolymers (Figure 9).[132,136,137,154] For example, in the study by White et al., a library of statistical copolymers with styrene, DOPA, and triethylamine repeating units were synthesized using free radical polymerization.[1] Since these copolymers are solid-like at room temperature with high glass transition temperatures (T_g > 80 ºC), they needed to be dissolved in a 90:10 mixture of chloroform:methanol to achieve effective spreading of the adhesive formulation in an aqueous environment. To initiate oxidative crosslinking of DOPA units, $Bu_4N^+(IO_4^-)$ was used as an oxidant in the adhesive formulation. The adhesive formulation showed A_{Lap} of ≈ 0.4 MPa when used to bond two Al_2O_3 substrates underwater. In the same study, the authors found that poly(vinyl acetate) and ethyl cyanoacrylate-based commercial glues showed negligible adhesion underwater. Interestingly, the incorporation of cationic groups in the polymer sidechain had a molar composition-dependent effect on the performance of the adhesive underwater. While the copolymer with 7% cation content showed the highest A_{Lap} of ≈ 0.4 MPa, the formulations with 0% and 16% cation content showed A_{Lap} of ≈ 0.18 and 0.15 MPa, respectively. White et al. suggested that the cationic groups are not the only reason for underwater adhesion, but may significantly contribute to bonding.[1] In a more recent study, the Wilker group designed a statistical copolymer with styrene and DOPA repeating units.[2] This styrene and DOPA copolymer with molar mass = 85 kDa with 20 mol% DOPA showed a maximum underwater tensile adhesion strength of ≈ 3 MPa to Al_2O_3 substrates submerged in seawater. Interestingly, the mussel byssal threads tested under the same conditions showed a tensile adhesion strength of ≈ 0.1 MPa only. Recently, the Wilker group reported an adhesive formulation that contains an acrylate-based copolymer with DOPA, methyl methacrylate, phosphate pendant groups, organic solvents

(chloroform and methanol), and $Bu_4N^+(IO_4^-)$ oxidant, that showed a maximum A_{Lap} of ≈ 0.5 MPa underwater.[69]

Other researchers have also developed adhesives based on DOPA copolymers. Sha et al. reported an alternating copolymer made of DOPA and bis(4-glycidyloxyphenyl) repeating units. An adhesive formulation of this alternating copolymer, organic solvents (chloroform and methanol), $FeCl_3$ (oxidant and crosslinker), showed A_{Lap} ≈ 0.9 MPa underwater.[152] Mu et al. tested the effect of polymer backbone and created four different variants of DOPA-conjugated polymers with increasing polarity of the polymer backbone.[22] Each adhesive formulation contained a copolymer with DOPA repeating units, organic solvents (methylene chloride and methanol), and crosslinking initiator ($FeCl_3$). In dry conditions, the A_{Lap} of three of the four polymers were identical. However, in the presence of water, the A_{Lap} increased as a function of the dielectric constant (polarity) of the polymer backbone. The adhesive formulation with poly(*N*-vinylpyrrolidone) backbone (highest dielectric constant) showed an A_{Lap} of ≈ 1.1 MPa while adhering to Al_2O_3 substrates in seawater.

Joy and Dhinojwala and coworkers demonstrated the importance of hydrophobic functional groups in addition to the DOPA groups in the design of underwater adhesives.[27,63,155] Xu et al. created a statistical copolyester composed of long aliphatic hydrocarbon, DOPA, and coumarin pendant groups.[27] Recognizing the importance of avoiding the use of organic solvents for *in vivo* applications, low viscosity copolyester adhesives with T_g < -50 ºC were designed from the above composition, allowing the adhesive to be applied underwater without the assistance of any solvents (Figure 9). The coumarin units in the copolyester undergo a photocycloaddition when exposed to UV light, which allows temporal and spatial control of the curing of the adhesive underwater. The copolyester adhesive was spread, cured, and tested underwater and showed a

maximum A_{Lap} of ≈ 0.65 MPa underwater. Interestingly, the authors found that the underwater adhesion was possible even in the absence of DOPA units. However, in the absence of hydrophobic functional groups, the underwater adhesion strength became negligible. Though the photo-crosslinking is very fast (< 10 min), at least one side of the substrate must be transparent for this formulation to be used. Kaur et al. showed that these hydrophobic adhesive elastomers form a patchy contact underwater.[63] The spectroscopic signals collected from the underwater contact of these elastomers suggest that DOPA is crucial in forming multimodal acid-base interactions with the substrate. However, the DOPA units do not displace interstitial water from the Al_2O_3 surface, and the hydrophobic groups help in displacing a significant amount of interstitial water. The combination of interstitial water displacement by hydrophobic groups and interfacial interactions at the dry patch of the patchy contact are the determining factors for the underwater adhesion of these mussel-inspired hydrophobic elastomers.[63] In a follow-up study, Narayanan et al. found that this copolyester adhesive showed 5-fold higher adhesion to porcine skin surface submerged in buffer compared to a commercial fibrin-based sealant.[155]

Another copolyester was developed by Jenkins et al., who created a biobased copolyester with methyl and DOPA pendant groups. This adhesive was applied underwater with the assistance of acetone:water mixture and oxidatively crosslinked with $Bu_4N^+IO4^-$ and it showed an A_{Lap} of ≈ 1.0 MPa underwater.[151] Both copolyester systems reported by Xu and Jenkins et al. are biodegradable and derived from renewable resources, making them environmentally friendly adhesives compared to most commercial adhesives.

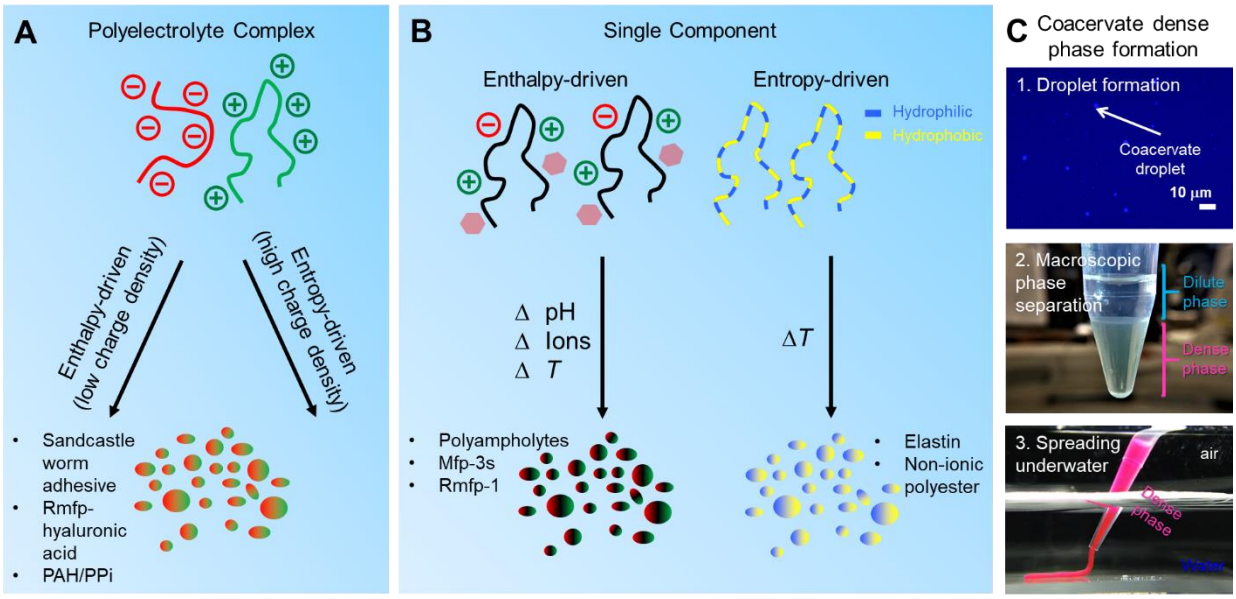

Figure 10. Most coacervating adhesive formulations are created from (A) polyelectrolyte complexation or (B) single component coacervation. In the polyelectrolyte complexes, the condensation between oppositely charged polyelectrolytes (enthalpic) or the release of counterions (entropy-driven) leads to phase separation. In the single-component coacervation, the enthalpic interaction between the functional groups or the entropy of hydration leads to phase separation. (C) Initially, the microscopic phase separation occurs creating coacervate droplets which later coalesce to form the distinct dilute and dense phases. The dense phase is typically used as the adhesive. The bottom panel shows the spreading of the coacervate dense phase underwater. Reproduced from ref. 24 with permission from the American Chemical Society, copyright 2011.

4.2 Synthetic Underwater Adhesive Coacervates

Most synthetic underwater adhesives reported in the literature consist of polymers with high storage moduli (> 1 MPa) and T_g > room temperature. Thus, they require the assistance of an organic solvent or a plasticizer to spread underwater. However, toxic plasticizers and organic solvents are harmful to the environment and are, thus, impractical for use in biomedical applications. Aquatic organisms, in contrast, use coacervation (i.e., LLPS) to overcome the challenge of spreading a relatively high modulus material underwater. The formation of a dense phase as a consequence of coacervation presents an elegant solution for spreading high moduli

proteins with water as a plasticizer. By mimicking this underwater adhesive delivery mechanism displayed by mussels and sandcastle worms, synthetic coacervating underwater adhesives have been created (Figure 10). Coacervating underwater adhesives have been fabricated from three classes of materials: (i) polyelectrolyte complexation (PECs): mixing of oppositely charged polymers (similar to mechanism used by the sandcastle worm), (ii) single-component coacervation (SCC): self-coacervation of polymers as a function of external stimuli such as temperature and salt concentration (similar to the process for Mfp-3s), and (iii) recombinant proteins: proteins synthesized using recombinant gene technology to exhibit coacervation through PEC or SCC mechanism.

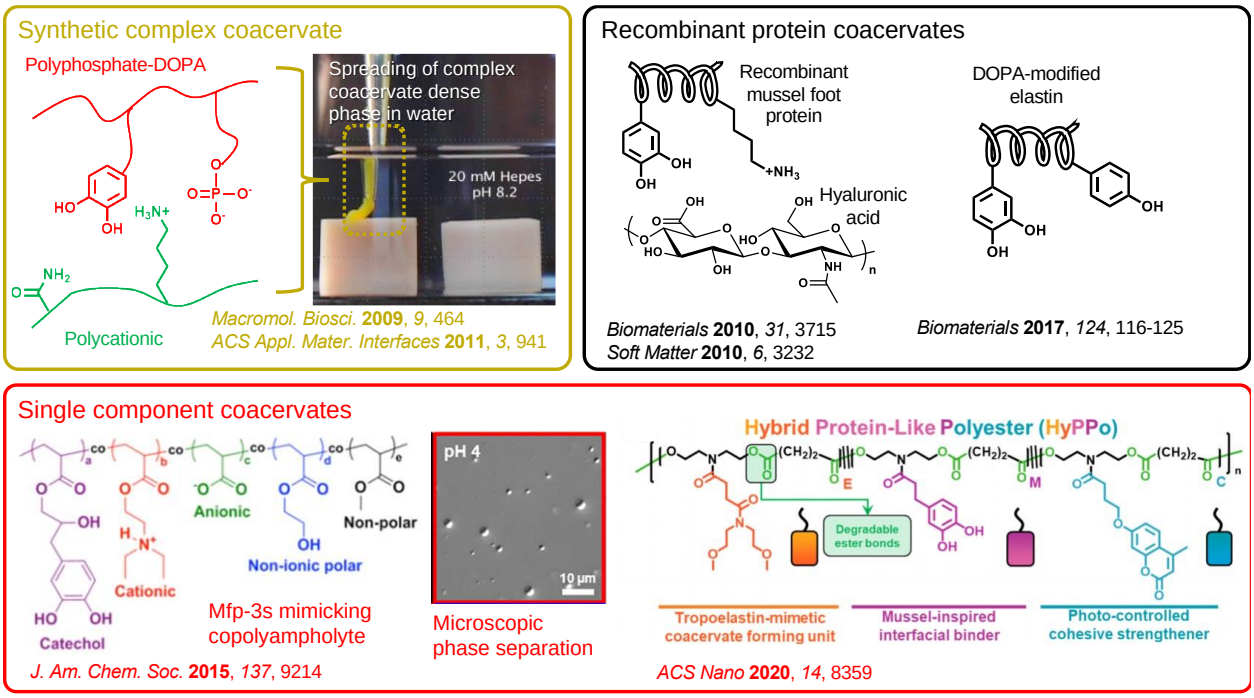

Figure 11. A few examples of coacervate underwater adhesives are shown here. Coacervates – the adhesive formulations that undergo a liquid-liquid phase separation process and a form dense phase. Synthetic coacervate underwater adhesives are formed from complex coacervation of polymers with opposite charges (yellow box), recombinant proteins (black box), and single component coacervates formed from polyampholytes and nonionic polyesters (red box).

Reproduced from ref. 30 with permission from the John Wiley and Sons, copyright 2009. Reproduced from ref. 146 with permission from the American Chemical Society, copyright 2015. Reproduced from ref. 24 with permission from the American Chemical Society, copyright 2021.

4.2.1 Synthetic polyelectrolyte complex coacervate underwater adhesives

Stewart and coworkers pioneered studies on sandcastle worm adhesives and theirs were among the first efforts to create a synthetic PEC adhesive formulation. In the first study by Shao et al., two oppositely charged copolyacrylates were made (Figure 11).[30] The first polymer resembled Pc3 with phosphate, acrylamide, and DOPA pendant groups and the second polymer resembled Pc1 with amine and acrylamide end groups. Mixing these two polymers in an aqueous solution at near-neutral pH resulted in PECs that separated into dense and dilute phases. The dense phase when oxidized with $NaIO_4$ showed an A_{Lap} of ≈ 0.25 MPa when used to bond together two bone specimens. In a follow-up study, the authors created an adhesive formulation with the dense phase formed from the PEC of the Pc3 analog and amine-terminated gelatin, Mg^{2+}, and $NaIO_4$.[25] The adhesive showed A_{Lap} of ≈ 0.75 MPa when adhering two Al_2O_3 substrates together. Kaur et al. further modified the adhesive formulation with dense phase formed from the PEC of Pc3 and Pc1, Ca^{2+}, PEG-diacrylate, $NaIO_4$, and polymerization initiators, which showed a remarkable A_{Lap} of ≈ 1 MPa when adhering to Al_2O_3 substrates.[21] Interestingly, the authors found that the adhesive formulation showed shear-thinning behavior, which aided in delivering the adhesive underwater through narrow nozzles. Although the underwater adhesives created by the Stewart group show strong adhesion underwater, the adhesives were not spread on the substrates underwater. Rather, the adhesive samples were prepared by applying the adhesives on the substrates outside water. In a more recent study, Lawrence et al. created two different PECs by mixing poly(allyl amine) (PAH) with pyrophosphate (PPi) or tripolyphosphate (TPP).[29] The underwater adhesion strength

of the dense phase formed from the PAH/PPi and PAH/TPP PECs showed a strong dependence on pH and ionic strength of the surrounding environment. For example, at pH = 7.0, the PAH/TPP complex showed an A_{Lap} of ≈ 0.4 MPa, which reduced to 0.05 MPa at pH = 6.0.

In other research, Kamperman and coworkers created PEC underwater adhesives from temperature-responsive cationic and anionic copolymers.[26,156–159] In the study by Dompé et al., a PEC formulation was prepared from a polyanionic polymer and a polycationic polymer each grafted with poly(N-isopropylacrylamide) (PNIPAM).[26] In aqueous solutions, PNIPAM shows a lower critical solution temperature (LCST) ≈ 32 ºC. Above 32 ºC, the PNIPAM segment of the copolymers dehydrates and increases the storage modulus of the adhesive.[160] The oppositely charged polymers grafted with PNIPAM were mixed near-neutral pH at room temperature, and the temperature was raised above the LCST upon which the solution transforms to a solid-like gel. The adhesion strength of this PNIPAM-based PEC was measured using a contact probe test.[161] A contact between glass and the PECs was made at 20 ºC and the temperature was raised to 50 ºC before pull-off. A maximum work of adhesion of 3.8 J/m^2 was obtained underwater by increasing the temperature. Notably, when the salt concentration was reduced, a roughly 3-fold increase in adhesion strength was observed compared to the sample where only the temperature was changed.[156]

Liquid-liquid phase separation behavior was recently observed while mixing polar organic molecules and polyoxometalates (POM).[162] Peng et al. observed that when silicotungstic acid was mixed with PEG, the mixture phase separates to form a dense phase similar to that of other reported coacervates. This dense phase showed a cohesive strength of ≈ 40 mJ/m^2 and an A_{Lap} of ≈ 70 kPa underwater.[163] Similar observation was reported by Li et al. in which the mixture between a short peptide and POM showed LLPS behavior.[164] The adhesive formulation showed an A_{Lap} of ≈ 30

kPa when adhering to stainless steel substrates underwater. Unlike other PECs, it is proposed that the hydrogen bonding between the polar organic molecule and POMs is responsible for the formation of LLPS in these systems.[163]

4.2.2 Synthetic single-component coacervate underwater adhesives

Inspired by the self-coacervation behavior of Mfp-3s, Seo et al. created acrylic copolyampholytes with varying molar ratios of polar, nonpolar, charged, and DOPA groups.[146] These copolyampholytes undergo a single-component coacervation behavior to form microdroplets (Figure 11). The copolyampholyte with a molar ratio of DOPA:cationic:anionic:polar:nonpolar = 30:6:4:51:9 showed an underwater adhesion strength of ≈ 39 mJ/m^2 when adsorbed to mica, which is nine-fold higher than that for Mfp-3s. However, the coacervates showed poor stability to changes in pH and ionic strength (only stable at pH between 4-5 and ionic strength < 20 mM) compared to Mfp-3s (stable at pH between 3-6 and ionic strength 100-600 mM). Ahn et al. simplified the design of the copolyampholytes with a DOPA-conjugated zwitterionic Gemini surfactant that undergoes LLPS. It was found that when treated with $NaIO_4$, the Gemini surfactant with a DOPA-head and 10 carbon tail showed an underwater adhesion strength of 50 mJ/m^2.[165] Kaminker et al. reported a simplistic Mfp-3s-inspired peptide sequence with 25 amino acid units that undergo self-coacervation in salty water. The dense phase formed from this coacervate deposited on an underwater surface showed underwater adhesion of ≈ 2 N/m without the assistance of any oxidants.[166]

Zhu et al. demonstrated a DOPA-free coacervating adhesive that can adhere to substrates in salty water.[167] They prepared a poly(amidoamine-epichlorohydrin) having an azetidinium cation with chloride (Cl^-) counterion. When this polymer was exposed to

bis(trifluoromethanesulfonyl)imide ($TFSI^-$) anion, the azetidinium cation exchanged the Cl^- with $TFSI^-$. Macroscopically, this counterion exchange transforms the initially clear polymer solution to a turbid liquid that later forms a dense phase. The authors suggest that this counterion exchange-induced coacervation is a unique approach for creating strong underwater adhesives (with $A_{Lap} \approx$ 80 kPa on glass substrates).

Most synthetic coacervates reported to date contain charged units, which result in a strong correlation between the pH or ionic strength and the physicochemical properties of the dense phase. Hence, adhesive formulations based on the adhesion of dense phases formed from PECs may not be applicable in a wet environment with a dynamic flow (as is the case for blood or physiologic fluids). Motivated by this unmet need in creating coacervate adhesives that are stable towards changes in pH and ionic strength, Narayanan et al. created non-ionic self-coacervating copolyesters.[24] These copolyesters were made from a temperature-responsive unit, DOPA, and coumarin. These copolyesters show liquid-liquid phase separation above their LCST. Due to the non-ionic nature of the copolyesters, the dense phase formation can be found in most ranges of pH (3-12) and ionic strength (0-1 M). Notably, these polyesters were spread, bonded, cured, and challenged underwater. The adhesives can be cured in less than 10 min and show a maximum adhesion strength of 0.1 MPa underwater. The authors suggested that the cytocompatibility, biodegradability, rapid curing, and insensitivity to environmental changes may position these polyesters to be useful for sealing tissue wounds even in the presence of blood.

4.2.3 Coacervating recombinant protein-based underwater adhesives

Purified adhesive proteins from nature are experimentally challenging to obtain in sufficient amounts for performing macroscopic adhesion measurements.[168] Hence, recombinant

genetic technology has been used to create proteins that mimic the structure of Mfp-3s.[169] Cha and coworkers created PECs from the complexation of cationic recombinant mussel foot protein (rmfp) and anionic hyaluronic acid.[147] This PEC showed an A_{Lap} of ≈ 0.2 MPa when adhering two aluminum sheets in wet conditions (100% humidity). Hwang et al. studied the interfacial and viscoelastic properties of the PECs created from rmfp (polycationic) and hyaluronic acid (polyanionic) using the surface force apparatus (SFA) (Figure 11).[122] It was found that the PECs showed shear-thinning properties and had low interfacial tension underwater. Hwang et al. suggested that the cation-π interactions in the rmfp are the dominant molecular interactions that lead to the LLPS behavior of rmfp. It was shown that a variant of this rmfp reported by Hwang et al. undergoes self-coacervation at a high salt concentration.[170] Also, this variant of rmfp undergoes LLPS in the presence of a cationic polymer (poly(2-(trimethylamino)ethyl methacrylate).[171] Both coacervating systems showed adhesive behavior underwater ($W_{ad} \approx 5.0$ mJ/m^2, measured with SFA on a mica surface).[170,171] Yang et al. reported a rmfp variant with high charge density that undergoes an enthalpy-driven upper critical solution temperature (UCST) behavior. They further showed that the adhesion behavior of this rmfp was elevated when the tyrosine units were modified to DOPA.[172]

Tropoelastin is a precursor of the mammalian protein elastin, which has an intrinsically disordered protein sequence with regions of alternating hydrophobic and hydrophilic amino acid residues.[173] Interestingly, tropoelastin shows LCST behavior in aqueous solutions, and above the LCST temperature it undergoes a single-component LCST-driven coacervation.[174] Brennan et al. created elastin-like polypeptides (ELPs) using recombinant gene expression technology.[28] These ELPs showed LCST behavior in water and formed a dense phase. After purification of the obtained protein, the authors converted the tyrosine units in the ELPs to DOPA using tyrosinase (Figure

11). Raising the temperature above LCST resulted in a dense-phase adhesive formulation of the DOPA-conjugated ELPs with an A_{Lap} of ≈ 0.2 MPa when adhering to Al_2O_3 substrates underwater.

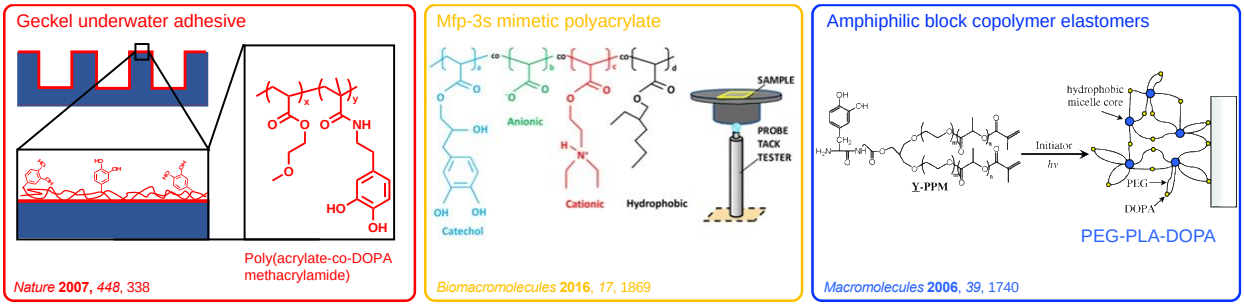

Figure 12. Some examples of tacky underwater adhesive materials. Tacky adhesives are mostly elastomer-like polymeric materials where the underwater adhesion is measured using a contact probe. Some of the popular examples of each class are provided. Reproduced from ref. 175 with permission from the American Chemical Society, copyright 2006. Reproduced from ref. 176 with permission from the American Chemical Society, copyright 2016.

4.3 DOPA-Conjugated Tacky Adhesives

Geckos are able to climb vertical walls by maximizing the contact area using miniature hairy adhesive structures found on their toe pad.[177] The reversible nature of the gecko toe pad adhesive has been mimicked using nanopatterned soft substrates.[178] However, these gecko-inspired nanopatterned adhesives show a significant reduction (3-fold) in adhesion when challenged to adhere to hydrophilic underwater surfaces.[179] To overcome this weak underwater adhesion of nanopatterned soft substrates, Lee et al. created a gecko-mussel-hybrid reversible adhesive named Geckel, that incorporates elements of both gecko and mussel adhesives (Figure 12).[180] Geckel is a nanopatterned PDMS surface that is coated with poly(dopaminemethacrylamide-*co*-methoxyethylacrylate). The coating of DOPA-conjugated polymer resulted in ≈ 7-fold increase in the underwater adhesion strength compared to the copolymer-free gecko-inspired adhesive. Tiu et

al. fabricated pressure-sensitive underwater adhesives using a similar polymer backbone. In this study, a library of polyacrylate copolymers was created with n-butylacrylate, DOPA, and anionic or cationic pendant groups.[31,71] The copolymer with n-butylacrylate:DOPA:anionic ratio of 80:5:10 (pendant groups) showed an underwater adhesion strength of ≈ 50 N/25 mm in a 180º peel test, which was not statistically different from its DOPA-free variant.[31]

Clancy et al. created acrylic copolymers with DOPA/phenyl, cationic, anionic, and hydrophobic groups that mimic Mfp-3s (which contains DOPA) and barnacle cement proteins (which contain phenyl instead of DOPA).[176] The adhesion strength of these copolymers was tested underwater using a tack adhesion geometry (Figure 12). The copolymer that was devoid of charged groups showed the highest underwater adhesion. Conspicuously, it was found that the barnacle cement mimetic copolymer (which used phenyl instead of DOPA) showed a higher underwater adhesion strength than the Mfp-mimetic copolymers in the presence or absence of charged species.

Lee et al. created a series of amphiphilic block copolymers with poly(ethylene oxide) (PEG), polylactic acid (PLA), and DOPA repeating units and methacrylate (MA) end groups.[175] In the presence of a photoinitiator and light, the aqueous solution of this MA-terminated triblock copolymer crosslinks to form a DOPA-conjugated hydrogel. A contact work of adhesion of 410 mJ/m^2 was required to separate the interface between this amphiphilic DOPA-hydrogel and Ti-surface underwater.

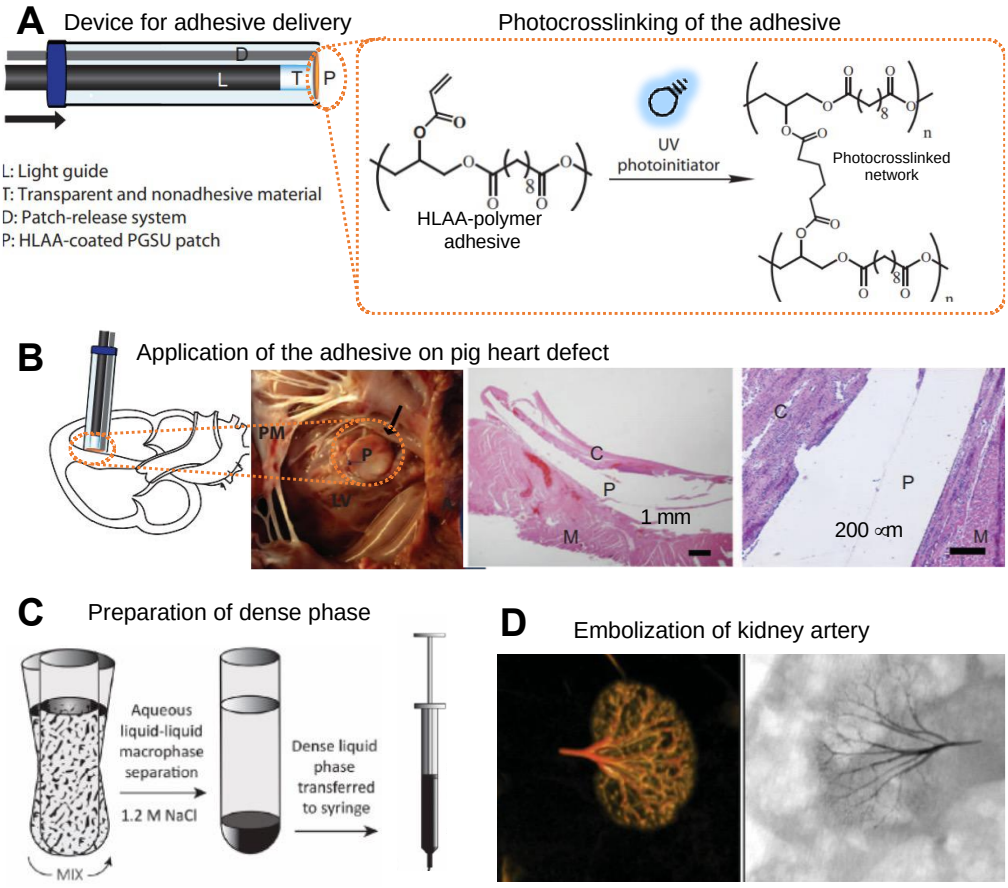

Figure 13. A few examples of biomedical applications of wet adhesives. (A) A light guide containing device is used for crosslinking and delivering bioinspired hydrophobic light-activated adhesive (HLAA)-polymer adhesive. The right side shows the photocrosslinking reaction through which the HLAA polymer crosslinks to create the viscoelastic network. Reproduced from ref. 9 with permission from the American Association for the Advancement of Science, copyright 2014. (B) The application of HLAA adhesive on a pig heart defect and the histological images that show the area of the adhesive-pericardium interface. (C) Application of a coacervate-based underwater adhesive for embolization of arteries. Preparation of the dense phase from protamine sulfate and sodium inositol hexaphosphate (left) and the (D) microscopic images of the embolized rabbit kidney artery. Reproduced from ref. 181 with permission from the WILEY-VCH Verlag GmbH & Co. KGaA, Weinheim, copyright 2016.

5.0 Summary

The past decade has witnessed a paradigm shift in the field of synthetic underwater adhesives due to the detailed research on adhesive mechanisms of aquatic organisms. In the previous sections, we highlighted several studies that demonstrated the ability of synthetic adhesives to spread, bond, cure in water, and resist water infiltration into the adhesive joint, all of which were once thought to be very difficult. These advances have positioned some of the bioinspired adhesives as potential replacements for current tissue sealants.[32,36–38,182,183] For example, Lang et al. created bioinspired blood-immiscible photocrosslinkable adhesives that act as a hemostatic glue as demonstrated in pigs with bleeding cardiac wounds (Figure 13A and Figure ***13***B).[9] In a different application, Jones et al. demonstrated the embolization of blood vessels in a rabbit kidney using a PEC system that solidifies in intravascular ionic concentrations (Figure 13C and Figure ***13***D).[181] Park et al. used the rmfp-hyaluronic acid PEC formulation developed by Cha and coworkers to improve the persistence of stem cells.[184] The authors found that fixing stem cells using the dense phase of the coacervates improved the multipotency and angiogenesis of stem cells. With the recent advancements in creating underwater adhesives, in the coming years, we anticipate that underwater adhesives will become an important tool in modern surgery,[7,32,33] biomaterial development,[6,185] soft robotics,[186,187] restoration of architecture and art, and high-performance coatings.

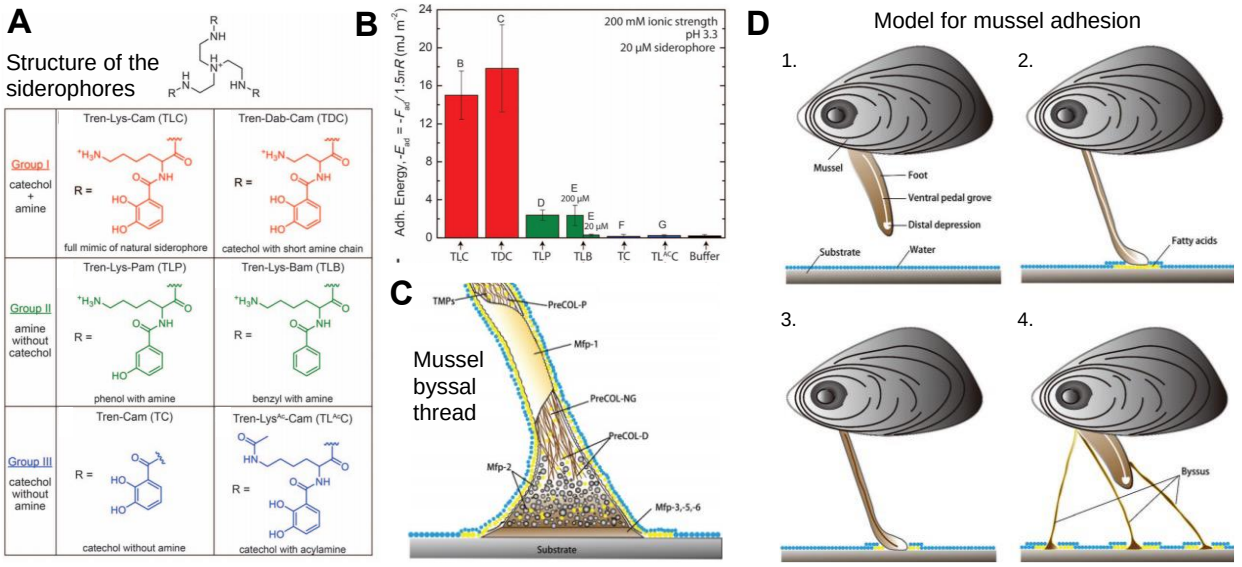

Figure 14. A summary of the underexplored pathways of mussel adhesion for creating underwater adhesives. (A) Chemical structures of the siderophores were created by mimicking the bacterial secretions. (B) The adhesion strength of the siderophores was measured using SFA against mica surfaces. The synergistic action between cationic and DOPA units helps to displace the interfacial ions and increase the adhesion strength. Reproduced from ref. 77 with permission from the American Association for the Advancement of Science, copyright 2015. (C) An updated schematic of the mussel byssal thread adhesive mechanism. The fatty acids found in the byssal thread are added to the scheme. (D) Proposed mechanism of mussel adhesion with the help of fatty acids. The authors propose that the fatty acids may help in removing the interstitial water before the protein deposition. Reproduced from ref. 188 with permission from the Royal Society of Chemistry, copyright 2018.

6.0 Future Directions

6.1 What More Can We Learn From Mussels?

Mussel-inspired adhesives have certainly set the path to creating underwater adhesives. However, there is much more to be translated from the mussel adhesion phenomena that will further help in designing synthetic adhesives with improved underwater adhesion. In a recent review, Herbert Waite wrote "*the reluctance of biotechnology to mimic anything but DOPA is unfortunate because mussels offer profound insights at multiple length scales and time scales for implementing wet adhesion*".[79] We believe that synthetic underwater adhesives have not yet advanced to the stage of our current understanding of mussel adhesion science. For example, other

than DOPA, interfacial Mfps are also rich in cationic lysine residues (Figure 6B). Using Mfp-mimetic dendrimers with DOPA-lysine siderophores, Maier et al. showed that the cationic groups can displace interstitial K^+ ions and water from mica surfaces (Figure 14A and Figure 14B).[77,189,190] It is proposed that once cationic groups are anchored on the substrate surface, DOPA groups form bidentate bonds more efficiently than the lysine-free siderophore variant. However, a conclusive correlation between the DOPA-lysine synergy and bulk adhesion strength was not found due to the influence of DOPA and lysine on both interfacial and cohesive interactions.[31,191–193]

Without water-free contact between the adhesive and substrate, underwater adhesion is impossible. Therefore, we propose that the design principles for the removal of interstitial water using DOPA-conjugated molecules require further scrutiny. While adsorbing onto a TiO_2 surface, a DOPA-conjugated Mfp-3s mimetic peptide was able to remove interstitial water more efficiently than the tyrosine variant.[108] However, Kaur et al. found that an elastomeric adhesive conjugated with DOPA does not remove interstitial water as compared to the acetonide-protected DOPA variant while adhering to Al_2O_3 underwater.[63] This suggests that DOPA molecules may require cooperativity from other amino acids or by other Mfp properties such as disordered protein structure, coacervation, or environmental design (pH or ionic strength regulation) to remove interstitial water. Interestingly, a recent study revealed that the mussel byssal thread and plaque are enriched with lipids.[188] From this unusual observation the authors suggested that the hydrophobic nature of the lipids helps to establish the initial contact to surfaces submerged in water (Figure 14C and Figure 14D) and the lipids are then expelled or adsorbed by the Mfps while transforming to the mature byssal thread. A combination of multiple adhesive mechanisms may help mussels remove interstitial water. Therefore, further research is required to understand how mussels drain the interstitial water with an assumption that the components in the adhesive plaque

may likely be more efficient in removing interstitial water than the Mfps found in the plaque core or byssal thread. A deeper understanding of the mechanisms that natural organisms use to repel interstitial water will substantially help in designing improved underwater adhesives.

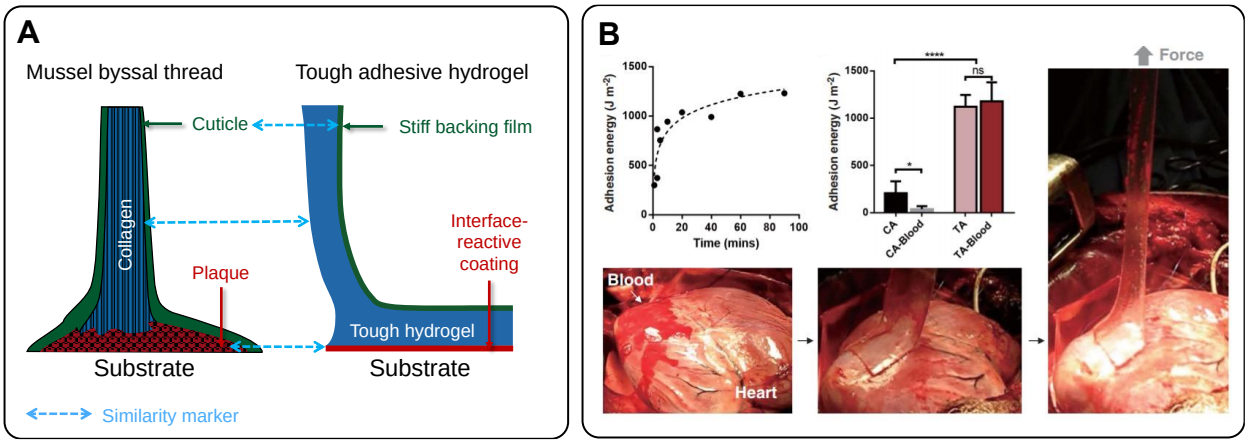

Figure 15. (A) The indirect relationship between the mussel adhesive holdfast (left) and the multilayer tough adhesives (right) developed by Zhao and coworkers.[194] The mussel adhesive cuticle, collagen, and plaque resemble the stiff backing, tough network, and interfacial layer of the multilayered adhesive. (B) The peel adhesion energy measurements of multilayer adhesives were demonstrated on a pig heart defect as a function of contact time (left) and their comparison to cyanoacrylate-based (CA) medical glue (right). The pictures on the bottom and right shows the application and adhesive nature of the tough adhesives on pig heart. Reproduced from ref. 195 with permission from the American Association for the Advancement of Science, copyright 2017.

An underexplored principle of mussel adhesion is the multicomponent hierarchical nature of the adhesive thread. For example, mussels secrete proteins that are specific for individual adhesive tasks such as surface priming (Mfp-3 and -5), viscoelastic dissipation (Mfp-1 and collagen), and protection (Mfp-1).[79] This task-oriented multi-component nature of the mussel byssal thread is rarely mimicked by adhesives described in the literature. An indirect example of a task-oriented multicomponent adhesive is the tough adhesive hydrogel created by Zhao and coworkers (Figure 15A).[72,194] The design of this adhesive consists of at least three layers: an interfacial layer designed

to react with the surface, a middle layer which is a multi-crosslinked tough network that is an excellent viscoelastic dissipator, and a top-most layer which is a high moduli plastic that protects the cohesive network from cracking.[194] In dry conditions, such adhesives show an interfacial toughness (similar to peel strength) of ≈ 1000 J/m^2. The Mooney and Zhao groups have independently demonstrated that such adhesives can be used for sealing wounds created in the internal organs of large animals (Figure 15B).[195–197]

The majority of mussel foot proteins show a disordered structure (Table 2). Such proteins with disordered regions have the propensity to phase separate in aqueous solutions.[198,199] For example, the single-component liquid-liquid phase separation behavior of Mfp-3s was recently documented.[123] The phase separation (e.g. coacervation) may help the proteins to spread onto surfaces submerged in water.[30,200,201] We suggest that molecular biologists and material scientists should study the proteomics of mussel foot proteins to understand the consequences of their disordered nature on phase separation behavior and underwater adhesion. Oftentimes, the phase separation is modulated in the presence of salt,[130] other disordered protein segments,[202] post-translational modifications,[203,204] and nucleic acids.[205] Since the Mfps are enriched with cationic and anionic residues in their molecular composition, cooperation between proteins is expected to modify their phase behavior. We think that understanding the cooperativity between mussel foot proteins to modulate their molecular and microscopic behavior will strengthen our understanding of mussel adhesion and inspire new multicomponent adhesive designs.

6.2 Where to Look for Further Inspirations?

Synthetic chemists and engineers can take inspiration for underwater adhesive designs from organisms other than mussels and sandcastle worms. For example, barnacles are proposed to show a unique method for adhering underwater.[85] While most of the mussel foot proteins have disordered structures, barnacle adhesive proteins consist of beta-sheet structures.[206] Recently, So et al. identified an alternating sequence between charged and simple amino acid domains in barnacle adhesive protein that only polymerizes and forms a fibrous network in the presence of another protein with an antiparallel structure.[207] Such molecular-level control over the formation of amyloid-like structures in barnacle adhesive sets forth a novel mechanism for the temporal control over the solidification of underwater adhesives. Using synthetic polymers that form secondary structures in response to a stimulus or secondary molecule, researchers may design barnacle-inspired glues that stick to surfaces using the amyloid-like fibrous adhesive networks.

Adhesives used by spiders have also been studied to explore their mechanism of adhesion in humid conditions. Spiders hunt in wet habitats and capture prey using sticky aggregate glue droplets whose adhesion is resistant to humid conditions.[208,209] These spider silk glue drops are a mixture of glycoproteins and low molecular weight inorganic and organic compounds.[208] Singla et al. propose that the low molecular weight, hygroscopic salts found in the spider silk glue droplets help in removing the interstitial water from hydrophilic surfaces by adsorbing water into the cohesive network of the glue.[210] Inspired by this mechanism, Yuk et al. improvised the wet adhesion of reactive tough hydrogel adhesives.[197] In this design, the tough hydrogels are dried under a vacuum. This dried hydrogel is proposed to act as a water adsorber and provide interfacial contact with wet surfaces. The dry tough hydrogel adhesives showed an A_{Lap} of ≈ 100 kPa when adhering to wet porcine skin.

6.3 Supramolecular Underwater Adhesives

Supramolecular underwater adhesives that do not mimic biological adhesives are also getting attention. For example, Liu et al. created nucleobase-containing organogels that show an A_{Lap} of ≈ 0.1 MPa when adhering to iron plates underwater.[211] An elegant example of supramolecular adhesion was shown by Li et al. in which a low molecular weight molecule was created with dibenzo-24-crown-8 building blocks.[212] The 4-arm version of this molecule shows a melting point ≈ 50 ºC. The melted material was deposited on surfaces submerged underwater. These supramolecular adhesives showed an A_{Lap} of ≈ 3 MPa while adhering steel plates underwater. A small-molecule adhesive was synthesized by Giuri et al. that adheres to substrates only when applied underwater.[213] The authors found that the protection of hydroxyl groups in the DOPA-conjugated molecule improved the underwater adhesion compared to the free-DOPA variant.

6.4 Challenges to Resolve in Underwater Adhesive Design, Testing, and Characterization

The transformation of an adhesive from a low viscous fluid that can spread on underwater surfaces to a solid-like cured structure usually relies on adhesive formulations that use toxic organic solvents as diluents (Table 4).[2,151] A proposed mechanism to overcome the dependence on solvents is to rely on polymers with low T_g and viscosity which can be crosslinked to create solid-like structures.[27] However, it is experimentally challenging to convert polymers with low viscosity to high Young's moduli polymers (typically to Young's modulus more than 1 MPa). Thus, maintaining wetting properties to enable efficient surface contact and later transforming to a high modulus adhesive underwater remains the central problem in creating underwater adhesives. The

use of supramolecular adhesives[212] and the phase inversion mechanism[79] observed in mussel adhesives (Figure 6C) may provide a solution to overcome this problem.

From section 4.0 of this review, one can understand that researchers are starting to resolve some of the outstanding challenges brought by water that prevent adhesion to surfaces submerged in water. Most of the substrates used in these studies are atomically or microscopically smooth,[2,21,27,94] even though the practical adhesive interfaces such as tires gripping the road, mussel byssal threads on rocks, geckos climbing the walls are rough in diverse length scales. Adhering to such rough surfaces underwater is an arduous task since rough surfaces have asperities that prevent the adhesive from wetting underwater. Such asperities reduce the adhesive-substrate contact and weaken the adhesive performance.[214] Interestingly, Bradley et al. found that when roughness was introduced to the adhesive hydrogel surfaces, they become more adhesive ($A_{\mathrm{Lap}} \approx 2.4$ kPa to polystyrene dish) to surfaces submerged in water compared to their smooth counterpart (no adhesion).[215] Wang et al. created a cupped bioinspired microstructure that sticks to rough surfaces underwater.[216] It was found that the instability caused by the roughness at the contact interface squeezes the water from the asperities of the substrate. The elastic force generated from the collapse of these asperities resisted the peeling of the cupped adhesive from the rough substrate. These two studies set a starting point for researchers to create adhesives for rough surfaces underwater. We believe that there needs to be a collective effort from physicists, engineers, and material scientists for improving our understanding of the adhesive contacts between rough surfaces underwater and design solutions to overcome the challenges brought by water and surface roughness.

It is impossible to find a single type of adhesion measurement technique that is suitable for measuring the adhesion strength of different types of adhesive materials. For example, the bulk

and coacervating polymer adhesives are tested using the lapshear adhesion strength measurements,[1,3,21,25,151] the pressure-sensitive adhesives are commonly tested with peel tests,[71,197,217] and the elastomeric and adsorbed polymers are tested using JKR model adhesion measurements.[63,96,218] Hence, the magnitude and units of adhesion strength vary significantly across different studies. If the authors are comparing their formulation with other adhesives, instead of reporting from other literature examples, we encourage the authors to test a few of the comparable adhesives in similar conditions as the newly created adhesive formulation. Also, this review calls for an initiative to develop experimental kits with protocols for underwater adhesion measurements. We believe that the errors caused by the variations in experimental conditions followed in different research labs can be minimized with the approaches suggested.

Future underwater adhesive designs should focus on overcoming the challenges brought on by interstitial water with a multitude of design principles. To achieve this, the characterization of the interface between the adhesive and substrate underwater is crucial. Experimental techniques such as ATR-IR,[108,219] sum-frequency generation spectroscopy,[63,64,133,220–222] interferometry,[96,165,223] and ODNP[109,201,224] are currently available to characterize the buried adhesive interfaces. However, due to the very few studies in this area, characterizing the interface between the adhesive and the underwater surface has been a tremendous experimental challenge and there is an urgent need for developing simple microscopic tools that characterize the underwater adhesive contacts.

Conflicts of Interest

The authors declare no conflicts.

Acknowledgement

The authors acknowledge funding from the National Science Foundation (NSF DMR Awards 1508440 and 1610483). Authors acknowledge Ms. Sheila L Pearson for technical editing assistance.

References

1 J. D. White and J. J. Wilker, *Macromolecules*, 2011, **44**, 5085–5088.

2 M. A. North, C. A. Del Grosso and J. J. Wilker, *ACS Appl. Mater. Interfaces*, 2017, **9**, 7866–7872.

3 K. Zhan, C. Kim, K. Sung, H. Ejima and N. Yoshie, *Biomacromolecules*, 2017, **18**, 2959–2966.

4 C. Wei, X. Zhu, H. Peng, J. Chen, F. Zhang and Q. Zhao, *ACS Sustain. Chem. Eng.*, 2019, **7**, 4508–4514.

5 A. H. Hofman, I. A. van Hees, J. Yang and M. Kamperman, *Adv. Mater.*, 2018, **30**, 1704640(1–38).

6 Q. Guo, J. Chen, J. Wang, H. Zeng and J. Yu, *Nanoscale*, 2020, **12**, 1307–1324.

7 W. D. Spotnitz, *Am. Surg.*, 2012, **78**, 1305–1321.

8 R. F. Reinoso, B. A. Telfer and M. Rowland, *J. Pharmacol. Toxicol. Methods*, 1997, **38**, 87–92.

9 N. Lang, M. J. Pereira, Y. Lee, I. Friehs, N. V. Vasilyev, E. N. Feins, K. Ablasser, E. D. O'Cearbhaill, C. Xu, A. Fabozzo, R. Padera, S. Wasserman, F. Freudenthal, L. S. Ferreira, R. Langer, J. M. Karp and P. J. Del Nido, *Sci. Transl. Med.*, 2014, **6**, 218ra6(1–10).

10 A. P. Duarte, J. F. Coelho, J. C. Bordado, M. T. Cidade and M. H. Gil, *Prog. Polym. Sci.*, 2012, **37**, 1031–1050.

11 L. P. Bré, Y. Zheng, A. P. Pêgo and W. Wang, *Biomater. Sci.*, 2013, **1**, 239–253.

12 J. H. Waite, *Int. J. Adhes. Adhes.*, 1987, **7**, 9–14.

13 M. K. Chaudhury and G. M. Whitesides, *Langmuir*, 1991, **7**, 1013–1025.

14 Sugiman and Sulardjaka, *Int. J. Technol.*, 2016, **7**, 438–446.

15 R. J. Stewart, T. C. Ransom and V. Hlady, *J. Polym. Sci. Part B Polym. Phys.*, 2011, **49**, 757–771.

16 J. H. Waite and M. L. Tanzer, *Science*, 1981, **212**, 1038–1040.

17 R. J. Stewart, J. C. Weaver, D. E. Morse and J. H. Waite, *J. Exp. Biol.*, 2004, **207**, 4727–4734.

18 K. Kamino, S. Odo and T. Maruyama, *Biol. Bull.*, 1996, **190**, 403–409.

19 A. M. Smith, *Biological adhesives, Second edition*, 2016.

20 B. K. Ahn, *J. Am. Chem. Soc.*, 2017, **139**, 10166–10171.

21 S. Kaur, G. M. Weerasekare and R. J. Stewart, *ACS Appl. Mater. Interfaces*, 2011, **3**, 941–944.

22 Y. Mu, X. Wu, D. Pei, Z. Wu, C. Zhang, D. Zhou and X. Wan, *ACS Biomater. Sci. Eng.*, 2017, **3**, 3133–3140.

23 Y. C. Chen and H. Yang, *ACS Nano*, 2017, **11**, 5332–5338.

24 A. Narayanan, J. R. Menefee, Q. Liu, A. Dhinojwala and A. Joy, *ACS Nano*, 2020, **14**, 8359–8367.

25 H. Shao and R. J. Stewart, *Adv. Mater.*, 2010, **22**, 729–733.

26 M. Dompé, F. J. Cedano-Serrano, O. Heckert, N. van den Heuvel, J. van der Gucht, Y. Tran, D. Hourdet, C. Creton and M. Kamperman, *Adv. Mater.*, 2019, **31**, 1808179 (1–6).

27 Y. Xu, Q. Liu, A. Narayanan, D. Jain, A. Dhinojwala and A. Joy, *Adv. Mater. Interfaces*, 2017, **4**, 1700506(1–6).

28 M. J. Brennan, B. F. Kilbride, J. J. Wilker and J. C. Liu, *Biomaterials*, 2017, **124**, 116–125.

29 P. G. Lawrence and Y. Lapitsky, *Langmuir*, 2015, **31**, 1564–1574.

30 H. Shao, K. N. Bachus and R. J. Stewart, *Macromol. Biosci.*, 2009, **9**, 464–471.

31 B. D. B. Tiu, P. Delparastan, M. R. Ney, M. Gerst and P. B. Messersmith, *ACS Appl. Mater. Interfaces*, 2019, **11**, 28296–28306.

32 D. W. R. Balkenende, S. M. Winkler and P. B. Messersmith, *Eur. Polym. J.*, 2019, **116**, 134–143.

33 V. Bhagat and M. L. Becker, *Biomacromolecules*, 2017, **18**, 3009–3039.

34 L. Li and H. Zeng, *Biotribology*, 2016, **5**, 44–51.

35 L. Li, W. Smitthipong and H. Zeng, *Polym. Chem.*, 2015, **6**, 353–358.

36 A. Narayanan, Y. Xu, A. Dhinojwala and A. Joy, *ChemEngineering*, 2020, **4**, 32.

37 R. D. O'Rorke, O. Pokholenko, F. Gao, T. Cheng, A. Shah, V. Mogal and T. W. J. Steele, *Biomacromolecules*, 2017, **18**, 674–682.

38 P. J. M. Bouten, M. Zonjee, J. Bender, S. T. K. Yauw, H. Van Goor, J. C. M. Van Hest and R. Hoogenboom, *Prog. Polym. Sci.*, 2014, **39**, 1375–1405.

39 W. Zhang, R. Wang, Z. M. Sun, X. Zhu, Q. Zhao, T. Zhang, A. Cholewinski, F. Yang, B. Zhao, R. Pinnaratip, P. K. Forooshani and B. P. Lee, *Chem. Soc. Rev.*, 2020, **49**, 433–464.

40 C. Cui and W. Liu, *Prog. Polym. Sci.*, 2021, **116**, 101388 (1–34).

41 X. Zhao, X. Chen, H. Yuk, S. Lin, X. Liu and G. Parada, *Chem. Rev.*, 2021, **121**, 4309–4372.

42 A. N. Gent, *Langmuir*, 1996, **12**, 4492–4495.

43 G. Amarpuri, C. Zhang, C. Diaz, B. D. Opell, T. A. Blackledge and A. Dhinojwala, *ACS Nano*, 2015, **9**, 11472–11478.

44 A. Dupré and P. Dupré, *Théorie mécanique de la chaleur*, Gauthier-Villars, 1869.

45 F. M. Fowkes, *Ind. Eng. Chem.*, 1964, **56**, 40–52.

46 J. D. van der Waals, *Over de Continuiteit van den Gas- en Vloeistoftoestand [On the continuity of the gas and liquid state]*, 1873.

47 W. H. Keesom and A. P. Keesom, *Physica*, 1935, **2**, 557–572.

48 P. Debye, *J. Soc. Chem. Ind.*, 1929, **48**, 1036–1037.

49 F. London, *Trans. Faraday Soc.*, 1937, **33**, 8–26.

50 F. M. Fowkes, *Tribol. Ser.*, 1981, **7**, 119–137.

51 C. J. van Oss, M. K. Chaudhury and R. J. Good, *Chem. Rev.*, 1988, **88**, 927–941.

52 A. Eddi, K. G. Winkels and J. H. Snoeijer, *Phys. Fluids*, 2013, **25**, 013102(1–10).

53 A. N. Gent and A. J. Kinlock, *J Polym Sci Part A-2 Polym Phys*, 1971, **9**, 659–668.

54 A. N. Gent and J. Schultz, *J. Adhes.*, 1972, **3**, 281–294.

55 O. Reynolds, *Philanthr. Trans. R. Soc.*, 1983, **177**, 135–217.

56 A. Dhinojwala and S. Granick, *Macromolecules*, 1997, **30**, 1079–1085.

57 Y. Wang, C. Dhong and J. Frechette, *Phys. Rev. Lett.*, 2015, **115**, 248302 (1–5).

58 A. V. Pocius, *Adhesion and adhesives technology: An introduction: Third edition*, 2012.

59 J. Israelachvili, *Intermolecular and Surface Forces*, 2011.

60 A. Nyarko, H. Barton and A. Dhinojwala, *Soft Matter*, 2016, **12**, 9132–9141.

61 A. P. Defante, A. Nyarko, S. Kaur, T. N. Burai and A. Dhinojwala, *Langmuir*, 2018, **34**, 4084–4094.

62 A. P. Defante, T. N. Burai, M. L. Becker and A. Dhinojwala, *Langmuir*, 2015, **31**, 2398–2406.

63 S. Kaur, A. Narayanan, S. Dalvi, Q. Liu, A. Joy and A. Dhinojwala, *ACS Cent. Sci.*, 2018, **4**, 1420–1429.

64 K. Nanjundiah, P. Y. Hsu and A. Dhinojwala, *J. Chem. Phys.*, 2009, **130**, 024702(1–7).

65 N. Dhopatkar, A. P. Defante and A. Dhinojwala, *Sci. Adv.*, 2016, **2**, e1600763.

66 American Society for Testing and Materials, ASTM D1002: Standard Test Method for Apparent Shear Strength of Single-Lap-Joint Adhesively Bonded Metal Specimens by Tension Loading (Metal-to-Metal), https://www.astm.org/Standards/D1002.htm, (accessed 20 July 2021).

67 L. F. M. da Silva, T. N. S. S. Rodrigues, M. A. V. Figueiredo, M. F. S. F. de Moura and J. A. G. Chousal, *J. Adhes.*, 2006, **82**, 1091–1115.

68 Y. Wang, X. Yang, G. Nian and Z. Suo, *J. Mech. Phys. Solids*, 2020, **143**, 103988 (1–16).

69 T. A. Jones and J. J. Wilker, *ACS Appl. Polym. Mater.*, 2020, **2**, 4632–4639.

70 ASTM International, ASTM D3330 / D3330M-04: Standard Test Method for Peel Adhesion of Pressure-Sensitive Tape, https://compass.astm.org/EDIT/html_annot.cgi?D3330+04(2018), (accessed 20 July 2021).

71 B. D. B. Tiu, P. Delparastan, M. R. Ney, M. Gerst and P. B. Messersmith, *Angew. Chemie - Int. Ed.*, 2020, **59**, 16616–16624.

72 H. Yuk, T. Zhang, S. Lin, G. A. Parada and X. Zhao, *Nat. Mater.*, 2016, **15**, 190–196.

73 H. Lee, N. F. Scherer and P. B. Messersmith, *Proc. Natl. Acad. Sci. U. S. A.*, 2006, **103**, 12999–13003.

74 S. Das, N. R. M. Rodriguez, W. Wei, J. H. Waite and J. N. Israelachvili, *Adv. Funct. Mater.*, 2015, **25**, 5840–5847.

75 A. D. Johnson, K. L.; Kendall, K.; Roberts, *Proc. R. Soc. London. A. Math. Phys. Sci.*, 1971, **324**, 301–313.

76 W. Wei, J. Yu, C. Broomell, J. N. Israelachvili and J. H. Waite, *J. Am. Chem. Soc.*, 2013, **135**, 377–383.

77 G. P. Maier, M. V. Rapp, J. H. Waite, J. N. Israelachvili and A. Butler, *Science*, 2015, **349**, 628–632.

78 Y. Li, Y. Li, T. Wang, L. Xia, L. Wang, M. Qin, W. Wang and Y. Cao, *J. Mater. Chem. B*, 2017, **5**, 4416–4420.

79 J. H. Waite, *J. Exp. Biol.*, 2017, **220**, 517–530.

80 K. W. Desmond, N. A. Zacchia, J. H. Waite and M. T. Valentine, *Soft Matter*, 2015, **11**, 6832–6839.

81 R. J. Stewart, C. S. Wang, I. T. Song and J. P. Jones, *Adv. Colloid Interface Sci.*, 2017, **239**, 88–96.

82 R. J. Stewart, C. S. Wang and H. Shao, *Adv. Colloid Interface Sci.*, 2011, **167**, 85–93.

83 K. Kamino, M. Nakano and S. Kanai, *FEBS J.*, 2012, **279**, 1750–1760.

84 K. P. Fears, B. Orihuela, D. Rittschof and K. J. Wahl, *Adv. Sci.*, 2018, **5**, 1700762(1–7).

85 C. Liang, J. Strickland, Z. Ye, W. Wu, B. Hu and D. Rittschof, *Front. Mar. Sci.*, 2019, **6**, 565.

86 N. Aldred and A. S. Clare, *Biofouling*, 2008, 24, 351–363.

87 K. Kamino, in *Biological Adhesives, Second Edition*, ed. A. M. Smith, Springer International Publishing, Cham, 2016, pp. 153–176.

88 H. G. Silverman and F. F. Roberto, *Mar. Biotechnol.*, 2007, **9**, 661–681.

89 L. Petrone, A. Kumar, C. N. Sutanto, N. J. Patil, S. Kannan, A. Palaniappan, S. Amini, B. Zappone, C. Verma and A. Miserez, *Nat. Commun.*, 2015, **6**, 8737.

90 G. M. Moeser and E. Carrington, *J. Exp. Biol.*, 2006, **209**, 1996–2003.

91 S. Altman and R. B. Whitlatch, *J. Exp. Mar. Bio. Ecol.*, 2007, **342**, 15–29.

92 B. P. Lee, P. B. Messersmith, J. N. Israelachvili and J. H. Waite, *Annu. Rev. Mater. Res.*, 2011, **41**, 99–132.

93 J. Yu, W. Wei, M. S. Menyo, A. Masic, J. H. Waite and J. N. Israelachvili, *Biomacromolecules*, 2013, **14**, 1072–1077.

94 J. Yu, Y. Kan, M. Rapp, E. Danner, W. Wei, S. Das, D. R. Miller, Y. Chen, J. H. Waite and J. N. Israelachvili, *Proc. Natl. Acad. Sci. U. S. A.*, 2013, **110**, 15680–15685.

95 J. Yu, W. Wei, E. Danner, R. K. Ashley, J. N. Israelachvili and J. H. Waite, *Nat. Chem. Biol.*, 2011, **7**, 588–590.

96 Q. Lin, D. Gourdon, C. Sun, N. Holten-Andersen, T. H. Anderson, J. H. Waite and J. N. Israelachvili, *Proc. Natl. Acad. Sci. U. S. A.*, 2007, **104**, 3782–3786.

97 Q. Lu, E. Danner, J. H. Waite, J. N. Israelachvili, H. Zeng and D. S. Hwang, *J. R. Soc. Interface*, 2013, **10**, 20120759(1–11).

98 M. Yu and T. J. Deming, *Macromolecules*, 1998, **31**, 4739–4745.

99 J. H. Waite and X. Qin, *Biochemistry*, 2001, **40**, 2887–2893.

100 S. W. Taylor, J. H. Waite, M. M. Ross, J. Shabanowitz and D. F. Hunt, *J. Am. Chem. Soc.*, 1994, **116**, 10803–10804.

101 C. J. Sun, A. Srivastava, J. R. Reifert and J. H. Waite, *J. Adhes.*, 2009, **85**, 126–138.

102 R. Mirshafian, W. Wei, J. N. Israelachvili and J. H. Waite, *Biochemistry*, 2016, **55**, 743–750.

103 E. W. Danner, Y. Kan, M. U. Hammer, J. N. Israelachvili and J. H. Waite, *Biochemistry*, 2012, **51**, 6511–6518.

104 T. H. Anderson, J. Yu, A. Estrada, M. U. Hammer, J. H. Waite and J. N. Israelachvili, *Adv. Funct. Mater.*, 2010, **20**, 4196–4205.

105 A. Narayanan, S. Kaur, N. Kumar, M. Tsige, A. Joy and A. Dhinojwala, *Macromolecules*, 2021, **54**, 5417–5428.

106 Y. Li, M. Qin, Y. Li, Y. Cao and W. Wang, *Langmuir*, 2014, **30**, 4358–4366.

107 P. Das and M. Reches, *Nanoscale*, 2016, **8**, 15309–15316.

108 W. Wei, L. Petrone, Y. Tan, H. Cai, J. N. Israelachvili, A. Miserez and J. H. Waite, *Adv. Funct. Mater.*, 2016, **26**, 3496–3507.

109 Y. Akdogan, W. Wei, K. Y. Huang, Y. Kageyama, E. W. Danner, D. R. Miller, N. R. Martinez Rodriguez, J. H. Waite and S. Han, *Angew. Chemie - Int. Ed.*, 2014, **53**, 11253–11256.

110 W. R. Wonderly, T. R. Cristiani, K. C. Cunha, G. D. Degen, J.-E. E. Shea and J. H. Waite, *Macromolecules*, 2020, **53**, 6767–6779.

111 M. A. Gebbie, W. Wei, A. M. Schrader, T. R. Cristiani, H. A. Dobbs, M. Idso, B. F. Chmelka, J. Herbert Waite and J. N. Israelachvili, *Nat. Chem.*, 2017, **9**, 473–479.

112 D. S. Hwang, H. Zeng, A. Masic, M. J. Harrington, J. N. Israelachvili and J. H. Waite, *J. Biol. Chem.*, 2010, **285**, 25850–25858.

113 E. Filippidi, T. R. Cristiani, C. D. Eisenbach, J. Herbert Waite, J. N. Israelachvili, B. Kollbe Ahn and M. T. Valentine, *Science*, 2017, **358**, 502–505.

114 Q. Li, D. G. Barrett, P. B. Messersmith and N. Holten-Andersen, *ACS Nano*, 2016, **10**, 1317–1324.

115 M. J. Harrington, A. Masic, N. Holten-Andersen, J. H. Waite and P. Fratzl, *Science*, 2010, **328**, 216–220.

116 L. A. Burzio and J. H. Waite, *Biochemistry*, 2000, **39**, 11147–11153.

117 B. Rost, *J. Struct. Biol.*, 2001, **134**, 204–218.

118 T. Williams, K. Marumo, J. H. Waite and R. W. Henkens, *Arch. Biochem. Biophys.*, 1989, **269**, 415–422.

119 D. S. Hwang and J. H. Waite, *Protein Sci.*, 2012, **21**, 1689–1695.

120 R. Van Der Lee, M. Buljan, B. Lang, R. J. Weatheritt, G. W. Daughdrill, A. K. Dunker, M. Fuxreiter, J. Gough, J. Gsponer, D. T. Jones, P. M. Kim, R. W. Kriwacki, C. J. Oldfield, R. V. Pappu, P. Tompa, V. N. Uversky, P. E. Wright and M. M. Babu, *Chem. Rev.*, 2014, **114**, 6589–6631.

121 S. Alberti, A. Gladfelter and T. Mittag, *Cell*, 2019, **176**, 419–434.

122 D. S. Hwang, H. Zeng, A. Srivastava, D. V. Krogstad, M. Tirrell, J. N. Israelachvili and J. H. Waite, *Soft Matter*, 2010, **6**, 3232–3236.

123 W. Wei, Y. Tan, N. R. Martinez Rodriguez, J. Yu, J. N. Israelachvili and J. H. Waite, *Acta Biomater.*, 2014, **10**, 1663–1670.

124 D. W. K. William F. Tanner, *SEPM J. Sediment. Res.*, 1968, **38**, 73–78.

125 H. Zhao, C. Sun, R. J. Stewart and J. H. Waite, *J. Biol. Chem.*, 2005, **280**, 42938–42944.

126 C. S. Wang and R. J. Stewart, *Biomacromolecules*, 2013, **14**, 1607–1617.

127 J. H. Waite, R. A. Jensen and D. E. Morse, *Biochemistry*, 1992, **31**, 5733–5738.

128 J. P. Buffet, E. Corre, E. Duvernois-Berthet, J. Fournier and P. J. Lopez, *Acta Biomater.*, 2018, **72**, 316–328.

129 V. S. Rathee, H. Sidky, B. J. Sikora and J. K. Whitmer, *J. Am. Chem. Soc.*, 2018, **140**, 15319–15328.

130 C. E. Sing and S. L. Perry, *Soft Matter*, 2020, **16**, 2885–2914.

131 M. J. Stevens, R. E. Steren, V. Hlady and R. J. Stewart, *Langmuir*, 2007, **23**, 5045–5049.

132 H. J. Meredith, C. L. Jenkins and J. J. Wilker, *Adv. Funct. Mater.*, 2014, **24**, 3259–3267.

133 J. Zhou, A. P. Defante, F. Lin, Y. Xu, J. Yu, Y. Gao, E. Childers, A. Dhinojwala and M. L. Becker, *Biomacromolecules*, 2015, **16**, 266–274.

134 V. Bhagat, E. O'Brien, J. Zhou and M. L. Becker, *Biomacromolecules*, 2016, **17**, 3016–3024.

135 S. Seo, D. W. Lee, J. S. Ahn, K. Cunha, E. Filippidi, S. W. Ju, E. Shin, B. S. Kim, Z. A. Levine, R. D. Lins, J. N. Israelachvili, J. H. Waite, M. T. Valentine, J. E. Shea and B. K. Ahn, *Adv. Mater.*, 2017, **29**, 1703026(1–9).

136 C. R. Matos-Pérez, J. D. White and J. J. Wilker, *J. Am. Chem. Soc.*, 2012, **134**, 9498–9505.

137 M. G. Mazzotta, A. A. Putnam, M. A. North and J. J. Wilker, *J. Am. Chem. Soc.*, 2020, **142**, 4762–4768.

138 Y. Zhang, X. Li, Q. Zhu, W. Wei and X. Liu, *Biomacromolecules*, 2020, **21**, 5222–5232.

139 G. Schmidt, B. R. Hamaker and J. J. Wilker, *Adv. Sustain. Syst.*, 2018, **2**, 1700159 (1–9).

140 Z. Wang, H. Kang, H. Liu, S. Zhang, C. Xia, Z. Wang and J. Li, *ACS Sustain. Chem. Eng.*, 2020, **8**, 16430–16440.

141 Y. Wei, J. Yao, Z. Shao and X. Chen, *ACS Sustain. Chem. Eng.*, 2020, **8**, 7668–7679.

142 H. Yamamoto, *J. Chem. Soc. Perkin Trans. 1*, 1987, 613–618.

143 A. Assmann, A. Vegh, M. Ghasemi-Rad, S. Bagherifard, G. Cheng, E. S. Sani, G. U.

Ruiz-Esparza, I. Noshadi, A. D. Lassaletta, S. Gangadharan, A. Tamayol, A. Khademhosseini and N. Annabi, *Biomaterials*, 2017, **140**, 115–127.

144 J. Shin, J. S. Lee, C. Lee, H. J. Park, K. Yang, Y. Jin, J. H. Ryu, K. S. Hong, S. H. Moon, H. M. Chung, H. S. Yang, S. H. Um, J. W. Oh, D. I. Kim, H. Lee and S. W. Cho, *Adv. Funct. Mater.*, 2015, **25**, 3814–3824.

145 E. Y. Jeon, B. H. Hwang, Y. J. Yang, B. J. Kim, B. H. Choi, G. Y. Jung and H. J. Cha, *Biomaterials*, 2015, **67**, 11–19.

146 S. Seo, S. Das, P. J. Zalicki, R. Mirshafian, C. D. Eisenbach, J. N. Israelachvili, J. H. Waite and B. K. Ahn, *J. Am. Chem. Soc.*, 2015, **137**, 9214–9217.

147 S. Lim, Y. S. Choi, D. G. Kang, Y. H. Song and H. J. Cha, *Biomaterials*, 2010, **31**, 3715–3722.

148 S. Moulay, *Polym. Rev.*, 2014, **54**, 436–513.

149 M. Yu, J. Hwang and T. J. Deming, *J. Am. Chem. Soc.*, 1999, **121**, 5825–5826.

150 M. J. Sever, J. T. Weisser, J. Monahan, S. Srinivasan and J. J. Wilker, *Angew. Chemie - Int. Ed.*, 2004, **43**, 448–450.

151 C. L. Jenkins, H. M. Siebert and J. J. Wilker, *Macromolecules*, 2017, **50**, 561–568.

152 X. Sha, C. Zhang, M. Qi, L. Zheng, B. Cai, F. Chen, Y. Wang and Y. Zhou, *Macromol. Rapid Commun.*, 2020, **41**, 2000055 (1–6).

153 A. Li, Y. Mu, W. Jiang and X. Wan, *Chem. Commun.*, 2015, **51**, 9117–9120.

154 G. Westwood, T. N. Horton and J. J. Wilker, *Macromolecules*, 2007, **40**, 3960–3964.

155 A. Narayanan, S. Kaur, C. Peng, D. Debnath, K. Mishra, Q. Liu, A. Dhinojwala and A. Joy, *Biomacromolecules*, 2019, **20**, 2577–2586.

156 M. Dompé, F. J. Cedano-Serrano, M. Vahdati, L. van Westerveld, D. Hourdet, C. Creton, J. van der Gucht, T. Kodger and M. Kamperman, *Adv. Mater. Interfaces*, 2020, **7**, 1901785(1–7).

157 M. Dompé, M. Vahdati, F. van Ligten, F. J. Cedano-Serrano, D. Hourdet, C. Creton, M. Zanetti, P. Bracco, J. van der Gucht, T. Kodger and M. Kamperman, *ACS Appl. Polym. Mater.*, 2020, **2**, 1722–1730.

158 M. Dompé, F. J. Cedano-Serrano, M. Vahdati, D. Hourdet, J. Van der Gucht, M. Kamperman and T. E. Kodger, *Polymers (Basel).*, 2020, **12**, 320.

159 M. Dompé, F. J. Cedano-Serrano, M. Vahdati, U. Sidoli, O. Heckert, A. Synytska, D. Hourdet, C. Creton, J. van der Gucht, T. Kodger and M. Kamperman, *Int. J. Mol. Sci.*, 2020, **21**, 100.

160 A. Narayanan, S. Chandel, N. Ghosh and P. De, *Anal. Chem.*, 2015, **87**, 9120–9125.

161 G. Sudre, L. Olanier, Y. Tran, D. Hourdet and C. Creton, *Soft Matter*, 2012, **8**, 8184–8193.

162 B. Jing, M. Ferreira, Y. Gao, C. Wood, R. Li, M. Fukuto, T. Liu and Y. Zhu, *Macromolecules*, 2019, **52**, 8275–8284.

163 Q. Peng, J. Chen, Z. Zeng, T. Wang, L. Xiang, X. Peng, J. Liu and H. Zeng, *Small*, 2020, **16**, 2004132(1–8).

164 X. Li, T. Zheng, X. Liu, Z. Du, X. Xie, B. Li, L. Wu and W. Li, *Langmuir*, 2019, **35**, 4995–5003.

165 B. K. Ahn, S. Das, R. Linstadt, Y. Kaufman, N. R. Martinez-Rodriguez, R. Mirshafian, E. Kesselman, Y. Talmon, B. H. Lipshutz, J. N. Israelachvili and J. H. Waite, *Nat. Commun.*, 2015, **6**, 8663 (1–7).

166 I. Kaminker, W. Wei, A. M. Schrader, Y. Talmon, M. T. Valentine, J. N. Israelachvili, J. H. Waite and S. Han, *Soft Matter*, 2017, **13**, 9122–9131.

167 X. Zhu, C. Wei, F. Zhang, Q. Tang and Q. Zhao, *Macromol. Rapid Commun.*, 2019, **40**, 1800758(1–7).

168 H. J. Kim, B. Yang, T. Y. Park, S. Lim and H. J. Cha, *Soft Matter*, 2017, **13**, 7704–7716.

169 J. Wang and T. Scheibel, *Biomacromolecules*, 2018, **19**, 3612–3619.

170 S. Kim, H. Y. Yoo, J. Huang, Y. Lee, S. Park, Y. Park, S. Jin, Y. M. Jung, H. Zeng, D. S. Hwang and Y. Jho, *ACS Nano*, 2017, **11**, 6764–6772.

171 S. Kim, J. Huang, Y. Lee, S. Dutta, H. Young Yoo, Y. Mee Jung, Y. Jho, H. Zeng and D. S. Hwang, *Proc. Natl. Acad. Sci. U. S. A.*, 2016, **113**, E847–E853.

172 B. Yang, S. Jin, Y. Park, Y. M. Jung and H. J. Cha, *Small*, 2018, **14**, 1803377(5–12).

173 S. E. Reichheld, L. D. Muiznieks, F. W. Keeley and S. Sharpe, *Proc. Natl. Acad. Sci. U. S. A.*, 2017, **114**, E4408–E4415.

174 S. G. Wise and A. S. Weiss, *Int. J. Biochem. Cell Biol.*, 2009, **41**, 494–497.

175 B. P. Lee, C. Y. Chao, F. Nelson Nunalee, E. Motan, K. R. Shull and P. B. Messersmith, *Macromolecules*, 2006, **39**, 1740–1748.

176 S. K. Clancy, A. Sodano, D. J. Cunningham, S. S. Huang, P. J. Zalicki, S. Shin and B. K. Ahn, *Biomacromolecules*, 2016, **17**, 1869–1874.

177 K. Autumn, Y. A. Liang, S. T. Hsieh, W. Zesch, W. P. Chan, T. W. Kenny, R. Fearing and R. J. Full, *Nature*, 2000, **405**, 681–685.

178 P. H. Niewiarowski, A. Y. Stark and A. Dhinojwala, *J. Exp. Biol.*, 2016, **219**, 912–919.

179 A. Y. Stark, I. Badge, N. A. Wucinich, T. W. Sullivan, P. H. Niewiarowski and A. Dhinojwala, *Proc. Natl. Acad. Sci. U. S. A.*, 2013, **110**, 6340–6345.

180 H. Lee, B. P. Lee and P. B. Messersmith, *Nature*, 2007, **448**, 338–341.

181 J. P. Jones, M. Sima, R. G. O'Hara and R. J. Stewart, *Adv. Healthc. Mater.*, 2016, **5**, 795–801.

182 M. Mehdizadeh and J. Yang, *Macromol. Biosci.*, 2013, **13**, 271–288.

183 I. Djordjevic, O. Pokholenko, A. H. Shah, G. Wicaksono, L. Blancafort, J. V. Hanna, S. J. Page, H. S. Nanda, C. B. Ong, S. R. Chung, A. Y. H. Chin, D. McGrouther, M. M. Choudhury, F. Li, J. S. Teo, L. S. Lee and T. W. J. Steele, *Biomaterials*, 2020, **260**, 120215.

184 T. Y. Park, E. Y. Jeon, H. J. Kim, B. H. Choi and H. J. Cha, *Acta Biomater.*, 2019, **86**, 257–268.

185 H. Zhang, T. Zhao, B. Newland, W. Liu, W. Wang and W. Wang, *Prog. Polym. Sci.*, 2018, **78**, 47–55.

186 P. Rao, T. L. Sun, L. Chen, R. Takahashi, G. Shinohara, H. Guo, D. R. King, T. Kurokawa and J. P. Gong, *Adv. Mater.*, 2018, **30**, 1801884.

187 K. C. Galloway, K. P. Becker, B. Phillips, J. Kirby, S. Licht, D. Tchernov, R. J. Wood and D. F. Gruber, *Soft Robot.*, 2016, **3**, 23–33.

188 Y. He, C. Sun, F. Jiang, B. Yang, J. Li, C. Zhong, L. Zheng and H. Ding, *Soft Matter*, 2018, **14**, 7145–7154.

189 M. V. Rapp, G. P. Maier, H. A. Dobbs, N. J. Higdon, J. H. Waite, A. Butler and J. N. Israelachvili, *J. Am. Chem. Soc.*, 2016, **138**, 9013–9016.

190 G. D. Degen, P. R. Stow, R. B. Lewis, R. C. Andresen Eguiluz, E. Valois, K. Kristiansen, A. Butler and J. N. Israelachvili, *J. Am. Chem. Soc.*, 2019, **141**, 18673–18681.

191 Y. Li, C. Liang, L. Gao, S. Li, Y. Zhang, J. Zhang and Y. Cao, *Mater. Chem. Front.*, 2017, **1**, 2664–2668.

192 M. Shin, J. Y. Shin, K. Kim, B. Yang, J. W. Han, N. K. Kim and H. J. Cha, *J. Colloid Interface Sci.*, 2020, **563**, 168–176.

193 H. Fan, J. Wang, Z. Tao, J. Huang, P. Rao, T. Kurokawa and J. P. Gong, *Nat. Commun.*, 2019, **10**, 5127(1–8).

194 T. Zhang, H. Yuk, S. Lin, G. A. Parada and X. Zhao, *Acta Mech. Sin. Xuebao*, 2017, **33**, 543–554.

195 J. Li, A. D. Celiz, J. Yang, Q. Yang, I. Wamala, W. Whyte, B. R. Seo, N. V. Vasilyev, J. J. Vlassak, Z. Suo and D. J. Mooney, *Science*, 2017, **357**, 378–381.

196 S. O. Blacklow, J. Li, B. R. Freedman, M. Zeidi, C. Chen and D. J. Mooney, *Sci. Adv.*, 2019, **5**, eaaw3963(1-9).

197 H. Yuk, C. E. Varela, C. S. Nabzdyk, X. Mao, R. F. Padera, E. T. Roche and X. Zhao, *Nature*, 2019, **575**, 169–174.

198 E. W. Martin and A. S. Holehouse, *Emerg. Top. Life Sci.*, 2020, **4**, 307–329.

199 K. You, Q. Huang, C. Yu, B. Shen, C. Sevilla, M. Shi, H. Hermjakob, Y. Chen and T. Li, *Nucleic Acids Res.*, 2020, **48**, D354–D359.

200 E. Spruijt, J. Sprakel, M. A. Cohen Stuart and J. Van Der Gucht, *Soft Matter*, 2009, **6**, 172–178.

201 K. Y. Huang, H. Y. Yoo, Y. Jho, S. Han and D. S. Hwang, *ACS Nano*, 2016, **10**, 5051–5062.

202 M. Feric, N. Vaidya, T. S. Harmon, D. M. Mitrea, L. Zhu, T. M. Richardson, R. W. Kriwacki, R. V. Pappu and C. P. Brangwynne, *Cell*, 2016, **165**, 1686–1697.

203 T. H. Kim, B. Tsang, R. M. Vernon, N. Sonenberg, L. E. Kay and J. D. Forman-Kay, *Science*, 2019, **365**, 825–829.

204 M. L. Nosella, M. Tereshchenko, I. Pritišanac, P. A. Chong, J. A. Toretsky, H. O. Lee and J. D. Forman-Kay, *J. Am. Chem. Soc.*, 2021, **143**, 11520–11534.

205 T. Kaur, M. Raju, I. Alshareedah, R. B. Davis, D. A. Potoyan and P. R. Banerjee, *Nat. Commun.*, 2021, **12**, 872.

206 M. Nakano and K. Kamino, *Biochemistry*, 2015, **54**, 826–835.

207 C. R. So, E. A. Yates, L. A. Estrella, K. P. Fears, A. M. Schenck, C. M. Yip and K. J. Wahl, *ACS Nano*, 2019, **13**, 5172–5183.

208 V. Sahni, T. A. Blackledge and A. Dhinojwala, *J. Adhes.*, 2011, **87**, 595–614.

209 B. D. Opell and M. L. Hendricks, *J. Exp. Biol.*, 2010, **213**, 339–346.

210 S. Singla, G. Amarpuri, N. Dhopatkar, T. A. Blackledge and A. Dhinojwala, *Nat. Commun.*, 2018, **9**, 1890.

211 X. Liu, Q. Zhang, L. Duan and G. Gao, *ACS Appl. Mater. Interfaces*, 2019, **11**, 6644–6651.

212 X. Li, Y. Deng, J. Lai, G. Zhao and S. Dong, *J. Am. Chem. Soc.*, 2020, **142**, 5371–5379.

213 D. Giuri, K. A. Jacob, P. Ravarino and C. Tomasini, *European J. Org. Chem.*, 2020, **2020**, 7144–7150.

214 S. Dalvi, A. Gujrati, S. R. Khanal, L. Pastewka, A. Dhinojwala and T. D. B. Jacobs, *Proc. Natl. Acad. Sci. U. S. A.*, 2019, **116**, 25484–25490.

215 L. C. Bradley, N. D. Bade, L. M. Mariani, K. T. Turner, D. Lee and K. J. Stebe, *ACS Appl. Mater. Interfaces*, 2017, **9**, 27409–27413.

216 Y. Wang and R. Hensel, *Adv. Funct. Mater.*, 2021, **31**, 2101787.

217 Y.-M. Tseng, A. Narayanan, K. Mishra, X. Liu and A. Joy, *ACS Appl. Mater. Interfaces*, 2021, **13**, 29048–29057.

218 C. Zhong, T. Gurry, A. A. Cheng, J. Downey, Z. Deng, C. M. Stultz and T. K. Lu, *Nat. Nanotechnol.*, 2014, **9**, 858–866.

219 D. E. Barlow, G. H. Dickinson, B. Orihuela, D. Rittschof and K. J. Wahl, *Biofouling*, 2009, **25**, 359–366.

220 C. Leng, Y. Liu, C. Jenkins, H. Meredith, J. J. Wilker and Z. Chen, *Langmuir*, 2013, **29**, 6659–6664.

221 C. Zhang, J. Jasensky, C. Leng, C. Del Grosso, G. D. Smith, J. J. Wilker and Z. Chen, *Opt. Lett.*, 2014, **39**, 2715.

222 C. A. Del Grosso, C. Leng, K. Zhang, H. C. Hung, S. Jiang, Z. Chen and J. J. Wilker, *Chem. Sci.*, 2020, **11**, 10367–10377.

223 M. Sun, N. Kumar, A. Dhinojwala and H. King, Adhesive forces inhibit underwater contact formation for a soft-hard collision, https://arxiv.org/abs/2102.10789, (accessed 21 July 2021).

224 İ. Kırpat, Y. Göksel, E. Karakuş, M. Emrullahoğlu and Y. Akdogan, *Mater. Lett.*, 2017, **205**, 48–51.